Electron Interactions with CCl_2F_2

L. G. Christophorou,[a] J. K. Olthoff, and Yicheng Wang[a]

National Institute of Standards and Technology, Electricity Division, Electronics and Electrical Engineering Laboratory, Gaithersburg, Maryland 20899-0001

Received February 21, 1997; revised manuscript received June 2, 1997

In this article, available information on the cross sections and rate coefficients for collisional interactions of dichlorodifluoromethane (CCl_2F_2) with electrons is critically evaluated and synthesized. This gas has many industrial uses and is of atmospheric and environmental interest. The CCl_2F_2 molecule fragments rather extensively under electron impact, principally via dissociative ionization and dissociative attachment; the latter process is temperature dependent. Information is presented and discussed on: (1) electron scattering processes [cross sections for total electron scattering, momentum transfer, differential elastic electron scattering, integral elastic electron scattering, and inelastic electron scattering for rotational and vibrational (direct and indirect) excitation]; (2) electron impact ionization (cross sections for total, partial, and double ionization and coefficients for electron impact ionization); (3) electron attachment (electron attachment cross sections and rate constants and their energy and temperature dependencies, electron attachment coefficients, dissociative attachment fragment anions, and negative ion states); (4) optical emission under electron impact, and (5) electron transport coefficients (electron drift velocity and ratio of transverse electron diffusion coefficient to electron mobility). Based upon the assessment of published experimental data, recommended values of various cross sections and rate coefficients are generated in graphical and tabular form. Areas where additional data are needed are identified, such as the measurement of the cross sections for momentum transfer and electron impact dissociation of CCl_2F_2 into neutral species. [S0047-2689(97)00205-5]

Key words: attachment; CCl_2F_2; cross sections; dichlorodifluoromethane; dissociation; electron interactions; fragments; ionization; scattering; transport.

Contents

[a]Also at the Department of Physics, The University of Tennessee, Knoxville, TN 37996.

List of Tables

List of Figures

1. Introduction

Dichlorodifluoromethane (CCl_2F_2) is an industrial gas, which was widely used as a refrigerant, a foam blowing agent, and an aerosol propellant. It is also a plasma processing gas[1] and has been used as an additive in gas dielectric mixtures. Dichlorodifluoromethane is of atmospheric and environmental interest because it is an ozone depleting gas due to solar photolysis releasing chlorine atoms which enter into catalytic stratospheric-ozone-depleting reactions.[2,3] Its residence time in the environment is about 102 years[4] and its global warming potential over a 100-year period has been reported to be 8500 compared[4] to the global warming potential of one for CO_2. Although CCl_2F_2 decomposes under low energy electron impact by dissociative ionization (Sec. 3) and by dissociative attachment (Sec. 6), to our knowledge these modes of decomposition of CCl_2F_2 have not been considered in studies aimed at the determination of its environmental impact. In this connection, it is worth noting that the electron impact decomposition of CCl_2F_2 and other chlorofluorocarbons via dissociative attachment processes increases considerably with increasing rovibrational excitation, that is, with increasing temperature. This may be of interest in its use in plasma reactors and in its environmental impact and removal from the environment.

Aspects of the electronic and molecular structure of CCl_2F_2 are discussed in Sec. 2 and the existing information on electron scattering cross sections (total, momentum transfer, differential elastic, integral elastic, and rotational and vibrational inelastic) are presented and discussed in Sec. 3. Electron impact ionization and dissociation processes are discussed in Secs. 4 and 5, respectively. Electron attachment coefficients, electron attachment cross sections and their energy and temperature dependencies, and dissociative attachment fragment anions are presented and discussed in Sec. 6. The limited data on electron transport coefficients are presented in Sec. 7, and optical emission from CCl_2F_2 under electron impact is covered in Sec. 8. Recommended cross sections and transport coefficients are given in Sec. 9, and the conclusions of the present work are summarized in Sec. 10.

The recommended cross sections and transport coefficients are derived from fits to the most reliable data that were available at the time of preparation of this article and they are not necessarily "final." The reliability of each set of data is determined by the following criteria:[5]

(i) data are published in peer reviewed literature;
(ii) no evidence of unaddressed errors;
(iii) data are absolute determinations;
(iv) multiple data sets are consistent with one another over ranges of overlap within combined stated uncertainties; and
(v) in regions where both experimentally and theoretically derived data exist, the experimental data are preferred.

In instances where only a single set of data for a given cross section or coefficient satisfies the above-mentioned criteria, that set is designated as our recommended set and is tabulated as originally published. In cases where two or more data sets satisfy the selection criteria, each selected data set is analyzed by a weighted-least-squares (WLS) fit, with the resulting data having an equal spacing of points. This is done in order to ensure that each selected data set is equally weighted in the final fit regardless of the number of points in

the original data. The recommended data set is then derived by a combined WLS fit to all of the data, and is presented in tabular and graphical format.

The collision cross sections, coefficients, and rate constants used in this work to quantify various electron collision processes are defined in Table 1 along with their corresponding symbols and units.

2. Electronic and Molecular Structure

The CCl_2F_2 molecule has C_{2v} symmetry. The valence shell independent-particle electronic configuration of the ground state can be written as:[6–8]

$(1a_1)^2\ (1b_1)^2\ (2a_1)^2\ (1b_2)^2\ (3a_1)^2\ (2b_2)^2\ (4a_1)^2\ (2b_1)^2\ (5a_1)^2\ (1a_2)^2\ (3b_1)^2\ (3b_2)^2\ (6a_1)^2\ (2a_2)^2\ (4b_1)^2\ (4b_2)^2\ ^1A_1$.

High resolution photoelectron spectroscopy[6,7] gives 12.26 eV, 12.53 eV, 13.11 eV, 13.45 eV, 14.36 eV, 15.9 eV, 16.30 eV, 16.9 eV, 19.3 eV, 20.4 eV, and 22.4 eV, for the vertical ionization energies of the outer valence orbitals $4b_2$, $4b_1$, $2a_2$, $6a_1$, $3b_2$, $3b_1$, $1a_2$, $5a_1$, $(2b_1 + 4a_1)$, $2b_2$, and $3a_1$, respectively. It has a dipole moment of 1.835×10^{-30} C m (0.55 D) (Ref. 9). Beran and Kevan[10] estimated three values (59.2×10^{-25} cm^3, 67.7×10^{-25} cm^3, and 64.3×10^{-25} cm^3) for the static polarizability of CCl_2F_2 using three different methods of calculation.

A number of workers investigated the electronic structure of the CCl_2F_2 molecule (see for example Refs. 6–8,11–16). Especially well investigated are the photoabsorption, photoionization, and photofragmentation properties of CCl_2F_2 (Refs. 2,7,11–14). In Fig. 1 the results of four photoabsorption cross section measurements[2,11–13] are compared with cross sections obtained from differential oscillator strength measurements using electrons with 100 eV (Ref. 17) and 8 keV (Ref. 6) energy. With the exception of the photoabsorption cross sections of Jochims *et al.*,[11] the rest of the data are in reasonable agreement. The data of Jochims *et al.* are described as absolute measurements with a quoted uncertainty of up to ±20%. The cross section determined from the differential oscillator strength data of Huebner *et al.*[17] was determined by normalization to the absorption cross section of Person *et al.*[18] at 12.22 eV and had a stated uncertainty of ±3%. Zhang *et al.*[6] pointed out that their technique has constant energy resolution [1 eV (full width at half maximum FWHM)] which is independent of the energy loss, whereas photoabsorption techniques have an energy resolution which becomes lower with increasing photon energy. This large difference in energy resolution complicates the comparison between the results obtained by their technique and the photoabsorption measurements. The absolute oscillator strength measurements of Zhang *et al.* are quoted with an uncertainty of ±5%. Above ~24 eV the data of Zhang *et al.*[6] are in agreement with the photoabsorption cross section values of Wu *et al.*[13] See further discussion and comparison with other data in Zhang *et al.*[6] Also see Refs. 6–8 and 11–16 for information on reactions, fragmentation patterns, energy positions, and cross sections for specific ions.

The electron energy-loss spectrum of CCl_2F_2 has been measured by King and McConkey[15] using electrons with 500 eV initial kinetic energy. Figure 2 shows the energy-loss spectrum of CCl_2F_2 obtained between 6 eV and 16 eV at 0° scattering angle. Table 2 lists the energy positions of the main features of the energy-loss spectrum as given by King and McConkey.[15] The energy positions of the main peaks are in good agreement with photoabsorption and other energy-loss studies.[11,14,18]

Table 3 lists the vertical ionization energies for CCl_2F_2. This molecule has four close-lying ionization thresholds due to ionization from the molecular orbitals formed by the chlorine lone pairs.[14] Their values are 12.3 eV, 12.6 eV, 13.2 eV, and 13.5 eV (Ref. 12). The vacuum ultraviolet (VUV) spectra up to 9.9 eV are also due to transitions from such orbitals.[12] The lowest CCl ionization onset is 14.4 eV (Ref. 12) although King and McConkey[15] argued that above 12 eV essentially all processes involve direct or dissociative ionization. Zhang *et al.*[6] showed that the ionization efficiency is equal to one for electron energies above ~17.5 eV.

Absolute dipole differential oscillator strengths for inner shell spectra have been determined by Zhang *et al.*[16] from high resolution energy-loss studies using electrons with 3 keV incident energy and zero degree mean scattering angle. They also measured absolute photoabsorption oscillator strengths in the equivalent photon energy range 8.5 eV–200 eV, and ionic photofragmentation branching ratios and the photoionization efficiency at equivalent photon energies from the first ionization threshold to 70 eV. Absolute partial photoionization oscillator strengths for dissociative photoionization have also been obtained by them.

The CCl_2F_2 molecule has nine nondegenerate fundamental vibrational modes, $\nu_1,\cdots,\nu_9$. Their energies, nuclear motion, symmetry, and infrared activity as summarized by Mann and Linder[19] are given in Table 4 (see, also, Shimanouchi[20]).

Dichlorodifluoromethane is an electronegative gas. Its electron attachment properties are discussed in Sec. 6. However, to aid the understanding of the electron scattering data from CCl_2F_2, we present here a summary of the work on the energies of the negative ion states of CCl_2F_2. The results obtained by various methods[21–39] are summarized in Table 5. The adiabatic electron affinity (EA) of CCl_2F_2 has been determined by Dispert and Lacmann[21] to be 0.4±0.3 eV using a potassium-atom beam to create the parent anion $CCl_2F_2^-$ via electron transfer in binary potassium-CCl_2F_2 collisions. A multiple scattering X_α calculation[22,23] has also given a positive value for the (EA) of the CCl_2F_2 molecule equal to 0.4 eV. A more recent quantum mechanical calculation[24] gave a value of 0.67 eV for the adiabatic electron affinity of CCl_2F_2.

Besides the potassium-atom charge exchange collision technique of Dispert and Lacmann,[21] five other types of experimental methods (threshold electron attachment technique,[25] swarm electron attachment technique,[26–30] electron beam/mass spectrometric techniques for electron attachment,[31–35] electron scattering,[36,37] and electron

TABLE 1. Definition of symbols

Symbol	Definition	Common scale and units
$\sigma_{sc,t}(\varepsilon)$	Total electron scattering cross section	10^{-20} m^2
$\sigma_{mt}(\varepsilon)$	Momentum transfer cross section	10^{-20} m^2
$\sigma_{e,diff}(\varepsilon)$	Differential elastic electron scattering cross section	10^{-20} m^2 sr^{-1}
$\sigma_{e,int}(\varepsilon)$	Integral elastic electron scattering cross section	10^{-20} m^2
$\sigma_{in}(\varepsilon)$	Inelastic electron scattering cross section	10^{-20} m^2
$\sigma_{rot,rovib,t}(\varepsilon)$	Cross section for pure rotational and rovibrational electron scattering	10^{-20} m^2
$\sigma_{vib,dir,t}(\varepsilon)$	Total direct vibrational excitation cross section	10^{-20} m^2
$\sigma_{in,indir,t}(\varepsilon)$	Total indirect inelastic electron scattering cross section	10^{-20} m^2
$\sigma_{non\text{-}ionizing,t}(\varepsilon)$	Nonionizing part of the total electron scattering cross section	—
$\sigma_{i,t}(\varepsilon)$	Total ionization cross section	10^{-20} m^2
$\sigma_{i,part}(\varepsilon)$	Partial ionization cross section	10^{-20} m^2
$\sigma_{i,double}(\varepsilon)$	Cross section for double ionization	10^{-22} m^2
$\sigma_{diss,neut,t}(\varepsilon)$	Total dissociation cross section into neutral species	10^{-20} m^2
σ_{em}	Emission cross section	10^{-23} m^2
$\sigma_{a,t}(\varepsilon)$	Total electron attachment cross section	10^{-20} m^2
$k_{a,t}$	Total electron attachment rate constant	10^{-10} cm^3 s^{-1}
$(k_{a,t})_{th}$	Thermal electron attachment rate constant	10^{-10} cm^3 s^{-1}
α/N	Density-reduced ionization coefficient	10^{-22} m^2
η/N	Density-reduced electron attachment coefficient	10^{-21} m^2
$(\alpha-\eta)/N$	Effective ionization coefficient	10^{-22} m^2
W	Average energy to produce an electron-ion pair	eV
w	Electron drift velocity	10^7 cm s^{-1}
D_T/μ	Transverse electron diffusion coefficient to electron mobility ratio	V
$\langle\varepsilon\rangle$	Mean electron energy	eV
$(E/N)_{lim}$	Limiting E/N value	10^{-21} V m^2

transmission[39]), and one calculation,[38] provided information on the negative ion states of CCl_2F_2. We have also determined the energies of the negative ion states of CCl_2F_2 from the positions of the maxima in the total indirect inelastic electron scattering cross section using data reported by Mann and Linder[19] (see Sec. 3).

The location of the negative ion states by the various methods are shown in Fig. 3. It should be noted that the positions of the negative ion states as determined from the resonance positions in electron attachment cross sections are normally lower than the corresponding energy positions determined from electron scattering due to the effect of autodetachment on the former process. In the last column of Fig. 3 are given the "average" positions of the negative ion states of CCl_2F_2 based on the data given in the figure. Clearly, on the basis of this figure, there exist at least five negative states above the zero level whose average energy positions are: −0.9 eV, −2.5 eV, −3.5 eV, −6.2 eV, and −8.9 eV. The −8.9 eV resonance lies in the region of electronic excitation (see Table 5) and most likely is associated with excited electronic states. The additional peak indicated by some experiments[26,27,35] at about −0.25 eV is questionable; its existence is indicated by two electron swarm[26,27] and one total attachment electron beam study,[35] but it is absent in the cross section of another similar beam study[31] and in electron scattering measurements (see Table 5). It may be associated with vibrationally excited molecules, but further work is needed to clarify the situation. The calculation of Underwood-Lemons *et al.*[38] located a state at −5.1 eV, but most likely this resonance is associated with that at −3.5 eV since no experimental evidence exists for a resonance at this energy from any other source and the calculation predicts four negative ion states which can be rationalized with the findings of other studies and molecular orbital assignments (see further discussion in Sec. 3).

3. Electron Scattering

3.1. General

In this section existing information is presented and discussed for the following electron collision cross sections: total electron scattering cross section, momentum transfer cross section, differential elastic electron scattering cross section, integral elastic electron scattering cross section, and inelastic electron scattering cross section for rotational and vibrational (direct and indirect) excitation.

The data are first presented to facilitate their comparison and they are subsequently evaluated and discussed. Recommended cross section values are given when possible. A model-based cross section set for CCl_2F_2 has been reported by Hayashi.[40] When possible, these cross sections are compared with experimental data in subsequent sections.

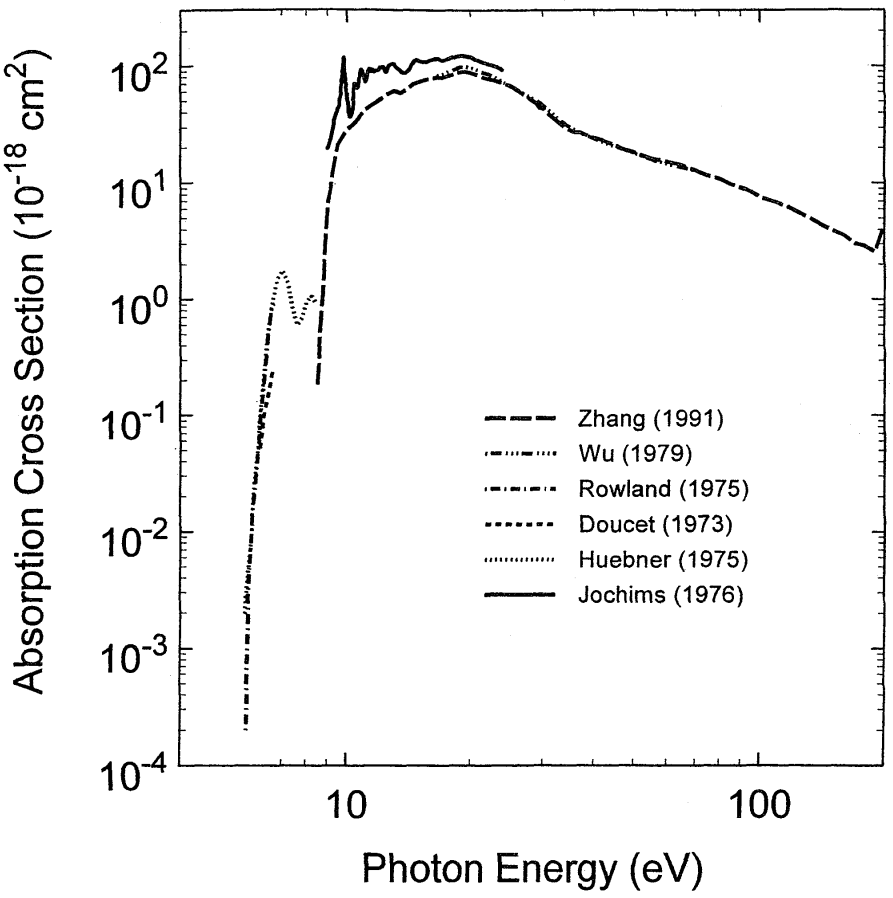

FIG. 1. Photoabsorption cross sections as a function of photon energy for CCl_2F_2. Photoabsorption studies: – . – (Ref. 2); — (Ref. 11); - - - (Ref. 12); — ... — (Ref. 13). Differential oscillator strength studies: .... (Ref. 17); — — (Ref. 6).

3.2. Total Electron Scattering Cross Section, $\sigma_{sc,t}(\varepsilon)$

There are two sets of measurements[37,38] of $\sigma_{sc,t}(\varepsilon)$ below 50 eV, one set of measurements[41] between 75 eV and 4000 eV, and one calculation[42] between 10 eV and 1000 eV. Figure 4 compares these data. The shapes of the two low-energy experimental sets[37,38] are nearly identical, but their magnitudes differ by about 25%, which is not within the combined quoted experimental uncertainty in the range from 0.7 –10 eV. Jones[37] quoted a most probable error of ±4.6% for energies <4.0 eV, about +4.5% and −4.2% for energies between 4.2 eV and 15.0 eV, +4.9% and −4.2% for energies between 16.0 eV and 25.0 eV, and +7.9% and −4.6% for energies between 26.0 eV and 50.0 eV. Underwood-Lemons *et al.*[38] do not explicitly quote the total uncertainty of their data, but indicate that two principal sources of error in determining the magnitude of the cross section in their experiments are the length of the electron trajectory through the target and the target number density. According to Underwood-Lemons *et al.* the former "introduces an uncertainty in the cross section of as much as 43% at 0.2 eV, declining to 17% at 0.5 eV, and to less than 10% above 1 eV," and the latter "implies an uncertainty of about ±11%." Zecca *et al.*[41] estimated their systematic errors to be less than ±3%. The calculation by Jiang *et al.*[42] employed the additivity rule and the complex optical potential and is not expected to give accurate results at low energies.

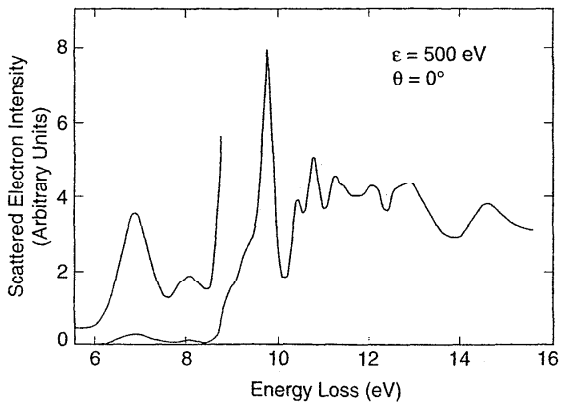

FIG. 2. Electron energy-loss spectrum of CCl_2F_2 at an incident electron energy of 500 eV and 0° scattering angle (from Ref. 15).

TABLE 2. Energies of peaks or shoulders, in eV, in the photoabsorption or energy-loss spectrum of CCl_2F_2

Ref. 15	Ref. 14	Ref. 11	Ref. 18[a]
6.95 (bp)[b]			
8.13 (bp)			
8.9 (s)	9.17 (s)		
9.35 (s)			
9.59 (s)			
9.77 (p)	9.81 (p)	9.8 (p)	
9.86 (s)			
10.45 (p)	10.46 (p)	10.5 (p)	
10.79 (p)	10.78 (p)	10.80 (p)	
11.29 (p)	11.29 (p)	11.24 (p)	
11.49 (p)		11.50 (p)	
11.75 (bp)		11.80 (p)	
12.06 (p)	12.10 (p)		12.10(p)
12.18 (s)			12.25(p)
12.64 (p)		12.6 (p)	
12.76 (p)	12.88 (p)	12.75 (p)	12.73(p)
12.93 (p)		12.90 (p)	12.95(p)
13.29 (s)			13.3 (s)
14.69 (bp)		14.70 (bp)	14.7(bp)
15.4 (bp)			15.4(bp)
16.34 (bp)		16.50 (bp)	16.0 (s)
			16.4(bp)
18.0 (s)			18.0 (s)
19.2 (bp)		19.20 (bp)	19.2(bp)
24.4 (bp)			
26.9 (bp)			

[a]As reported in Ref. 15.
[b]The symbols p, bp, and s, indicate peak, broad peak, and shoulder in the spectra.

Clearly, the calculated cross sections are much larger than the experimental data below about 80 eV, but are in reasonable agreement with the measurements of Zecca *et al.*[41] above this energy.

The experimental data of Jones[37] and Zecca *et al.*,[41] and the calculated values of Jiang *et al.*[42] (above 100 eV) were least squares fitted and the resultant cross section is shown in Fig. 4 by the solid line. Between 0.7 eV and 10 eV, the values of Jones[37] were used, rather than those of Underwood-Lemons *et al.*[38] because Jones' data have lower stated uncertainties and the Underwood-Lemons *et al.* data are lower than the sum of $\sigma_{e,\,int}$ (Fig. 7 later in this section) and $\sigma_{vib,\,dir,\,t}$ (Fig. 9 later in this section). Also, there seems to be a tendency of the $\sigma_{sc,\,t}(\varepsilon)$ data of Moore and collaborators to be consistently lower than other measurements at low energies [e.g., see data on CF_4 (Ref. 5), CHF_3 (Ref. 43), and SF_6 (Ref. 44)]. Below 0.7 eV the shape of the Underwood-Lemons's total electron scattering cross section was used to extend the fitted data down to 0.2 eV. Values for the fitted cross section curve are listed in Table 6 as our presently recommended values of $\sigma_{sc,\,t}(\varepsilon)$ for CCl_2F_2.

TABLE 3. Vertical ionization energies of CCl_2F_2, in eV, obtained from photoelectron data

Ref. 11	Ref. 12	Ref. 7[a]	Assignment (Refs. 12 and 14)
12.25	12.3	12.26	Cl lone pair
12.50	12.6	12.53	Cl lone pair
13.20	13.2	13.11	Cl lone pair
13.50	13.5	13.45	Cl lone pair
14.35	14.4	14.36	Lowest C–Cl molecular orbital
16.25		15.9	
		16.30	
		16.9	
19.2		19.3	
20.0		20.4	
		22.4	

[a]Vertical ionization energies of the outer valence orbitals.

TABLE 4. Vibrational modes of CCl_2F_2[a]

Mode	Energy (meV)	Nuclear motion	Symmetry	Activity
ν_1	136.1	CF_2 symmetric stretch	A_1	IR
ν_2	82.7	CF_2 bending	A_1	IR
ν_3	56.6	CCl_2 symmetric stretch	A_1	
ν_4	32.5	CCl_2 bending	A_1	IR
ν_5	39.9	torsion	A_2	
ν_6	144.7	CF_2 asymmetric stretch	B_1	IR
ν_7	55.3	CF_2 plane rocking	B_1	
ν_8	114.4	CCl_2 asymmetric stretch	B_2	IR
ν_9	53.9	CCl_2 plane rocking	B_2	

[a]Reference 19.

3.3. Momentum Transfer Cross Section, $\sigma_m(\varepsilon)$

There are no measurements of the momentum transfer cross section of CCl_2F_2. There have been only two calculations of $\sigma_m(\varepsilon)$ using the two-term approximation to the Boltzmann equation and various swarm and beam data.[40,45] The results of these calculations are presented in Fig. 5. Clearly an experimental determination of $\sigma_m(\varepsilon)$ is needed. In the absence of any experimental data, we do not designate any values as "recommended."

3.4. Differential Elastic Electron Scattering Cross Section, $\sigma_{e,\,diff}(\varepsilon)$

Mann and Linder[19] and Rohr[46] measured cross sections for vibrationally elastic electron-CCl_2F_2 scattering. Figure 6 compares their results for a 60° scattering angle. The pronounced minimum at ~0.5 eV has been interpreted[19] as a Ramsauer–Townsend minimum in the elastic channel. Randell *et al.*,[47] however, give the position of the Ramsauer–Townsend minimum around 0.04–0.06 eV (see later in this section).

The differential cross sections of Mann and Linder[19] for elastic electron-CCl_2F_2 scattering are listed in Table 7. The measurements clearly show that the cross section for elastic scattering in the forward direction increases with increasing electron energy.

TABLE 5. Energies, E_{NIS}, of the negative ion states of CCl_2F_2

Energy (eV)	Method	Reference
0.4 ± 0.3	Potassium-atom beam technique	21
0.4	Multiple scattering X_α calculation	22, 23
0.67	Quantum mechanical calculation	24
~0.0	Threshold attachment technique	25
<-0.1 ~-0.18 (shoulder) -1.05	Swarm-unfolded total attachment cross sections using N_2 as the buffer gas	26
-0.07 -0.30 -0.93	Swarm-unfolded total attachment cross section using N_2 as the buffer gas	27
~0 -0.8 -3.8	Swarm-unfolded total attachment cross section using N_2 and Ar as buffer gases	28
~0.0 ~-0.7 ~-3.5	Energies where the total attachment rate constant measured in N_2 and Ar buffer gases shows maxima	29,30
~0.0 ~-0.6 -3.5	Electron beam measurement of the total attachment cross section	31
-0.55 (Cl^-) -0.65 (Cl_2^-) -2.85 (FCl^-) -3.1 (F^-) -3.55 ($CFCl_2^-$) The energy dependence of the sum of all negative ions gives peaks at -0.6 eV and at -3.2 eV	Mass spectrometric study of dissociative attachment using a trochoidal monochromator	32–34
~0.0 -0.3 -0.95 -3.6	Mass spectrometric study of dissociative attachment using a trochoidal monochromator	35
-0.7 (Cl^-) -3.2 (F^-) -3.7 ($CFCl_2^-$)	ICR study of dissociative attachment	36
-1.0 -2.6 -4.0 -5.9	Total electron scattering cross section measurements	37
-1.2 -3.4 -4.6 -6.4	Estimates[a] of resonance energies determined from electron scattering experiments	38
-0.8 -3.1 -5.1 -6.7	Theoretical estimates[b]	38
-0.98 -2.35 -3.88	Vertical electron affinity values determined by electron transmission spectroscopy	39
-1.0 -2.5 -4.0 -6.0 -9.0	Maxima in the total indirect inelastic electron scattering cross section	Present analysis based on the work of Mann and Linder (Ref. 19): See Fig. 12 in Sec. 3

[a]Taken from Fig. 5 of Ref. 38.
[b]Calculated term values taken from Fig. 5 of Ref. 38.

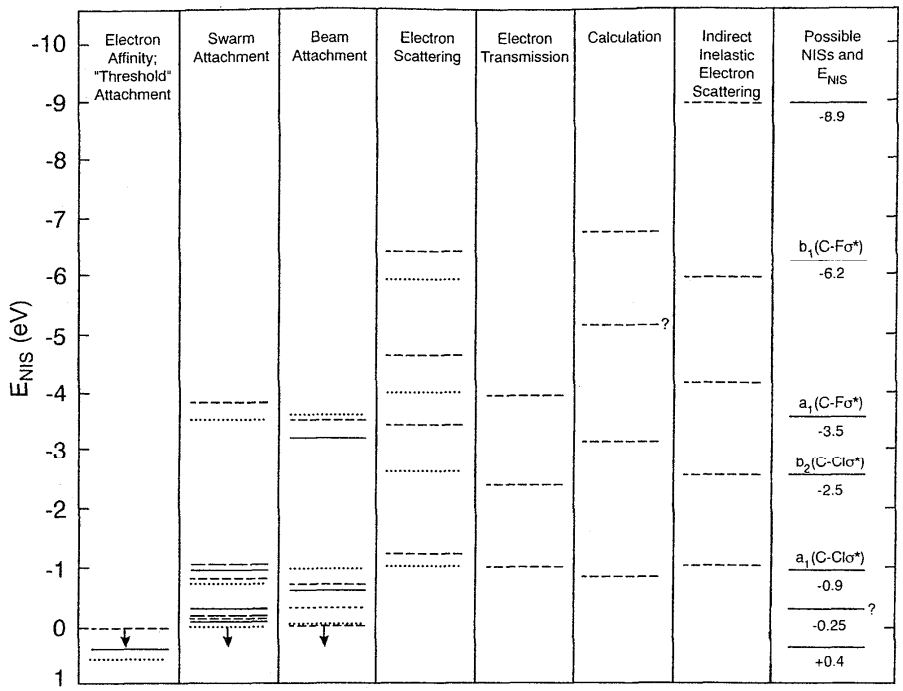

FIG. 3. Energy positions of the negative ion states of CCl_2F_2 below ~10 eV as obtained by various methods. Column 1: - - - [threshold attachment technique (Ref. 25)]; solid line [potassium-atom charge-exchange collision technique (Ref. 21) and calculation (Refs. 22 and 23)]; . . . , [calculation (Ref. 24)]. Column 2: Electron swarm attachment techniques: - - - (Ref. 28); ..... (Ref. 29); — — (Ref. 26); — (Ref. 27). Column 3; Electron beam attachment techniques: - - - (Ref. 31); — (Ref. 32); . . . (Ref. 35). Column 4: Electron scattering: .... (Ref. 37); - - - (Ref. 38). Column 5: Electron transmission: - - - (Ref. 39). Column 6: Calculation: - - - (Ref. 38). Column 7: Indirect inelastic electron scattering: - - - (present, see text). Column 8: Possible negative ion states and their energies and assignments (see text).

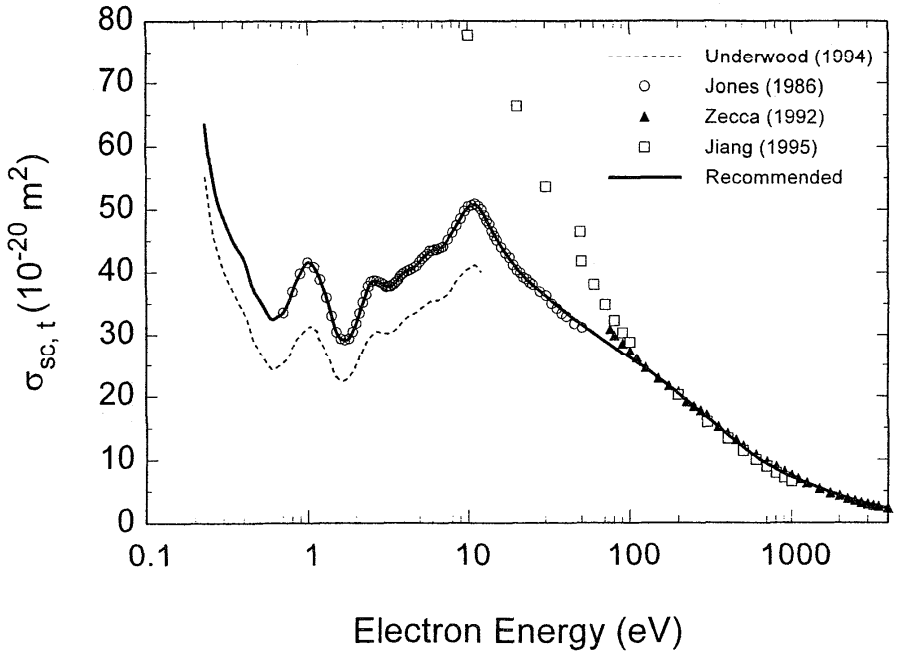

FIG. 4. Total electron scattering cross section, $\sigma_{sc,t}(\varepsilon)$, for CCl_2F_2. Experimental: - - - (Ref. 38); ○ (Ref. 37); ▲ (Ref. 41). Calculated: □ (Ref. 42). Recommended: —.

TABLE 6. Recommended $\sigma_{sc,t}(\varepsilon)$ for CCl_2F_2

Energy (eV)	$\sigma_{sc,t}(\varepsilon)(10^{-20}$ m$^2)$
0.23	63.5
0.3	48.6
0.35	44.6
0.4	42.2
0.45	38.1
0.5	35.5
0.6	32.5
0.7	33.6
0.8	36.9
0.9	39.8
1.0	41.5
1.5	30.5
2.0	31.8
2.5	38.5
3.0	38.0
3.5	38.2
4.0	39.9
4.5	40.6
5.0	41.6
6.0	43.4
7.0	44.1
8.0	46.3
9.0	48.5
10.0	50.5
12.5	49.0
15.0	45.3
20.0	40.5
25.0	38.0
30.0	36.2
35.0	34.7
40.0	33.5
45.0	32.5
50.0	31.6
60.0	30.1
70.0	28.9
80.0	27.9
90.0	27.0
100	26.2
150	23.0
200	20.4
250	18.3
300	16.6
350	15.1
400	13.9
450	12.8
500	11.9
600	10.4
700	9.4
800	8.5
900	7.7
1000	7.3
2000	4.3
3000	3.0
4000	2.2

3.5. Integral Elastic Electron Scattering Cross Section, $\sigma_{e,int}(\varepsilon)$

Mann and Linder[19] obtained the integral elastic electron scattering cross section, $\sigma_{e,int}(\varepsilon)$, by extrapolating their differential elastic cross sections (Table 7), weighted by sin θ, towards 0° and 180°. Their $\sigma_{e,int}(\varepsilon)$, taken from Fig. 3 of their article,[19] is shown here in Fig. 7. Numerical values from a fit to their data are listed in Table 8. Interestingly, $\sigma_{e,int}(\varepsilon)$ is structureless in this energy range although the total scattering cross section $\sigma_{sc,t}(\varepsilon)$ shows distinct structure due to the negative ion states in this energy range (see Fig. 4). As noted by Mann and Linder, the structure in the total electron scattering cross section is due to inelastic electron scattering (see Sec. 3.6).

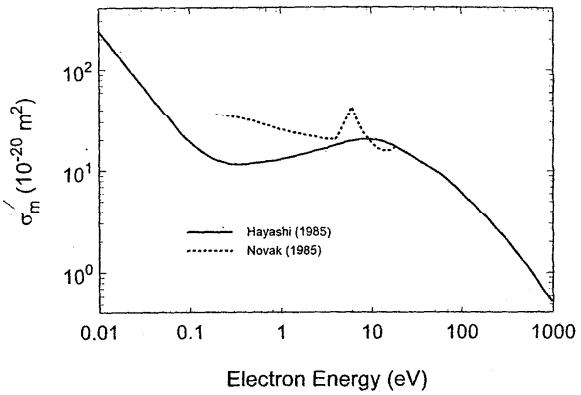

FIG. 5. Momentum transfer cross section, $\sigma_m(\varepsilon)$, as a function of electron energy for CCl_2F_2. Calculated values: — (Ref. 40); - - - - (Ref. 45).

3.6. Inelastic Electron Scattering Cross Section, $\sigma_{in}(\varepsilon)$

The CCl_2F_2 molecule has nine nondegenerate vibrational modes (Table 4) and shows significant vibrational excitation by electron impact at low energies. Furthermore, due to its permanent electric dipole moment, it has considerable rota-

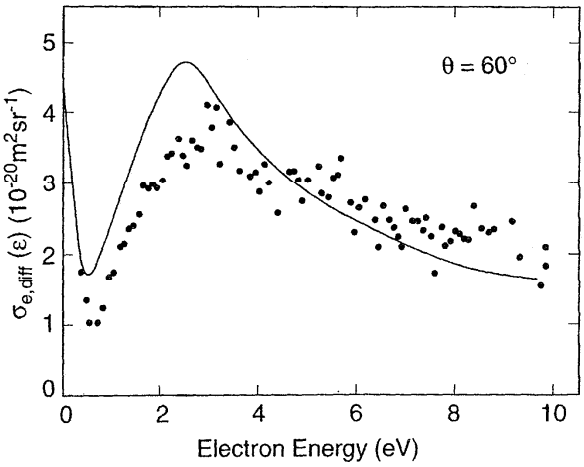

FIG. 6. Differential electron scattering cross section, $\sigma_{e,diff}(\varepsilon)$, as a function of electron energy for CCl_2F_2. — — (data of Rohr, Ref. 46, as quoted in Mann and Linder, Ref. 19); ● (data of Mann and Linder, Ref. 19).

TABLE 7. Differential cross sections, $\sigma_{e,diff}(\varepsilon)$, for elastic electron scattering from CCl_2F_2 in units of 10^{-20} m^2 sr^{-1}[a]

Energy (eV)	Scattering angle (deg)								
	20°	30°	40°	50°	60°	70°	80°	90°	100°
0.5	3.98	3.07	2.20	1.67	1.21	0.80	0.79	0.80	0.73
1.0	3.38	2.27	1.80	1.67	1.69	1.79	1.83	1.76	1.65
1.5	2.62	2.34	2.39	2.74	2.58	2.40	2.30	1.71	1.61
2.0	3.48	2.92	3.29	3.67	3.18	2.69	2.48	1.73	1.60
2.5	5.30	3.61	4.21	4.33	3.55	2.73	2.44	1.73	1.67
3.0	7.39	4.25	4.83	4.71	3.68	2.59	2.32	1.69	1.74
3.5	9.57	4.73	5.14	4.97	3.55	2.42	2.19	1.66	1.80
4.0	11.38	5.11	5.34	5.20	3.30	2.29	2.12	1.66	1.87
4.5	12.23	5.52	5.57	5.35	3.11	2.22	2.11	1.66	1.89
5.0	13.13	5.99	5.78	5.28	2.99	2.18	2.12	1.69	1.89
5.5	13.52	6.57	5.83	5.03	2.86	2.12	2.16	1.73	1.91
6.0	13.32	7.37	5.74	4.76	2.66	2.03	2.24	1.76	1.96
6.5	13.93	8.25	5.79	4.53	2.49	1.93	2.35	1.78	2.04
7.0	15.46	8.57	5.86	4.35	2.38	1.86	2.47	1.80	2.10
7.5	16.83	8.43	5.74	4.14	2.30	1.81	2.52	1.81	2.13
8.0	18.26	8.14	5.55	3.81	2.23	1.81	2.48	1.77	2.13
8.5	20.23	8.02	5.44	3.48	2.14	1.82	2.46	1.71	2.15
9.0	22.31	8.10	5.32	3.17	1.98	1.81	2.41	1.65	2.24
9.5	24.56	8.07	5.23	3.01	1.83	1.75	2.35	1.59	2.49

[a]See Ref. 19.

TABLE 8. Integral elastic electron scattering cross section, $\sigma_{e,int}(\varepsilon)$, for CCl_2F_2[a]

Energy (eV)	$\sigma_{e,int}(\varepsilon)(10^{-20}$ m$^2)$
0.5	14.7
0.6	15.8
0.7	16.9
0.8	18.0
0.9	19.0
1.0	20.0
1.5	24.1
2.0	27.2
2.5	30.2
3.0	32.6
3.5	34.4
4.0	35.7
4.5	36.7
5.0	37.4
6.0	38.2
7.0	39.9
8.0	40.8
9.0	42.6

[a]Data from Ref. 19.

tional excitation. Both, rotational and vibrational excitation are enhanced by indirect electron scattering through negative ion resonances.[47]

3.6.1. Rotational Excitation

The work of Randell *et al.*[47] on very-low-energy electron scattering by CCl_2F_2 has shown pure rotational excitation and rovibrational excitation for this molecule. Figure 8 shows the cross section for pure rotational and rovibrational electron scattering they deduced from their "backward scattering cross section" measurements and the adiabatic-rotation approximation under a number of assumptions.[47] The rapid rise below 0.1 eV has been attributed by Randell *et al.*[47] to pure rotational scattering and the cross section between 0.1 eV and 0.2 eV to threshold rovibrational excitation. The rovibrational scattering is weaker than the pure rotational scattering. Their analysis indicated the existence of a weak Ramsauer–Townsend (R-T) minimum at about 40–60 meV. According to Randell *et al.* the broad minimum around 500 meV, observed by Mann and Linder[19] (see Fig. 6) is "due to the tail of the rovibrational scattering cross section joining to the rise in the cross section associated with the shape resonance at ~1 eV." Thus, according to Randall *et al.*[47] the R-T minimum lies at a much lower energy than indicated by the data of Mann and Linder.[19]

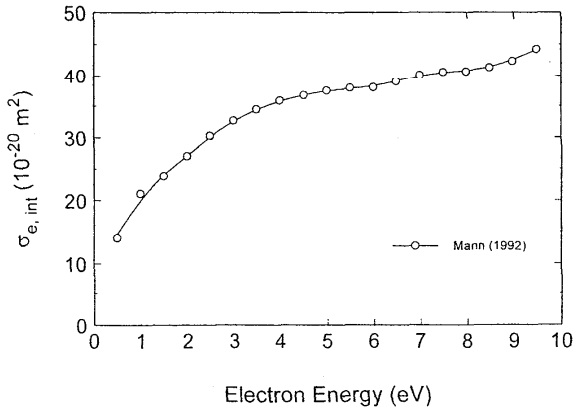

FIG. 7. Integral elastic electron scattering cross section, $\sigma_{e,int}(\varepsilon)$, for CCl_2F_2. (Data from Fig. 3 of Mann and Linder, Ref. 19.)

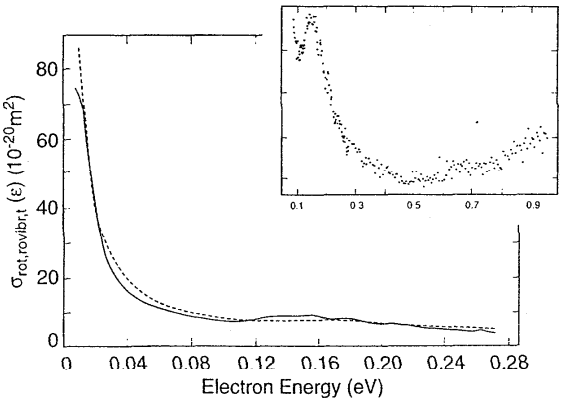

FIG. 8. Cross section for pure rotational and rovibrational electron scattering, $\sigma_{rot,rovibr}(\varepsilon)$, for CCl_2F_2. The experimental data (—) were arbitrarily scaled to fit the theoretical value (- - -) at 10 meV (Randell *et al.*, Ref. 47). The insert shows the scattering cross section (in arbitrary units) to 0.95 eV (from Randell *et al.*, Ref. 47, see this reference for details on the determination of these cross sections).

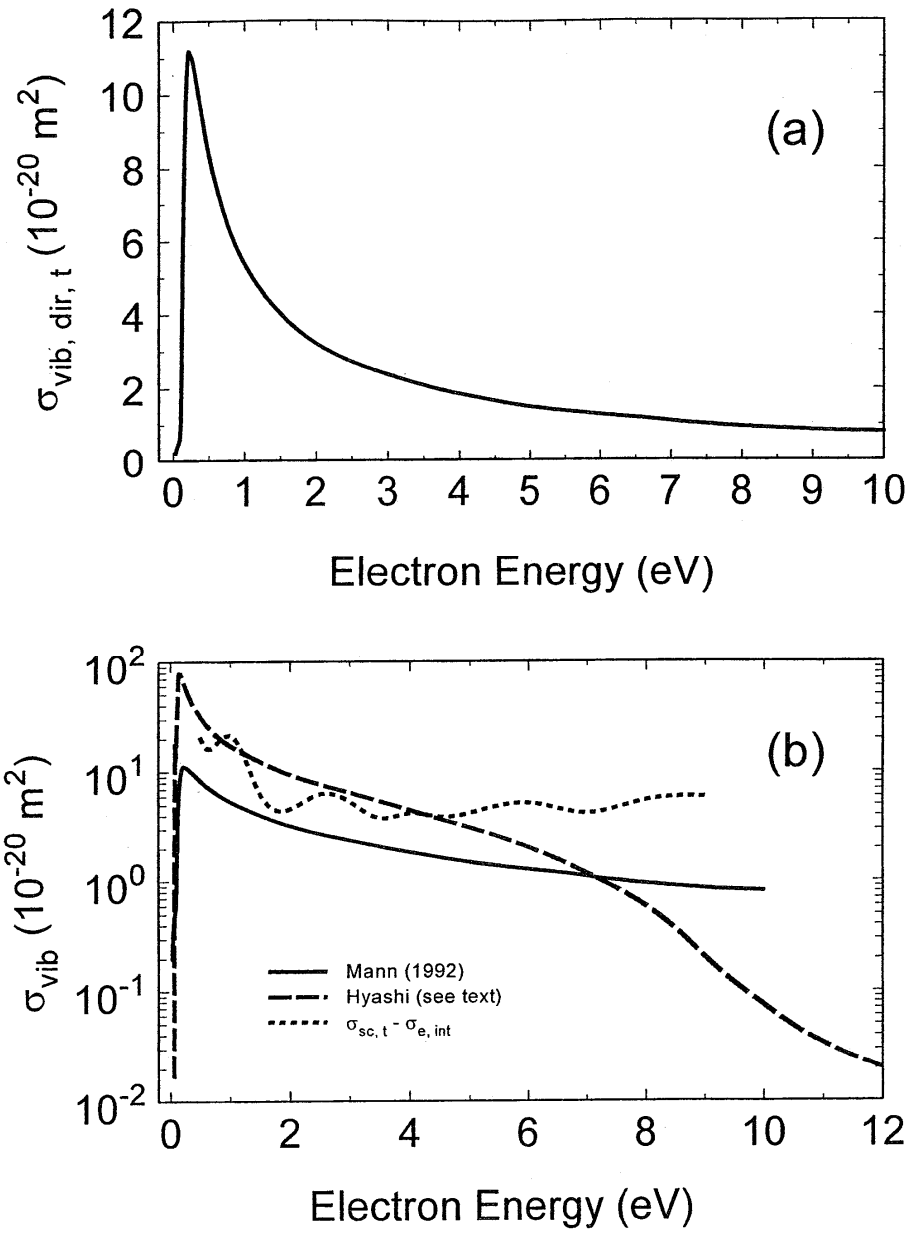

FIG. 9. (a) Born dipole approximation for the total direct vibrational excitation cross section, $\sigma_{vib, dir, t}(\varepsilon)$, for CCl_2F_2; sum of $\nu_1, \nu_2, \nu_4, \nu_6$, and ν_8 (derived from Fig. 3 of Mann and Linder, Ref. 19). (b) Comparison of vibrational excitation cross sections; —, $\sigma_{vib, dir, t}(\varepsilon)$; from Fig. 9 (a); - - -, $\sigma_{sc, t}(\varepsilon) - \sigma_{e, int}(\varepsilon)$ [determined using the values of $\sigma_{sc, t}(\varepsilon)$ and $\sigma_{e, int}(\varepsilon)$ in Tables 6 and 8, respectively]; — —, $\sigma\nu_3(\varepsilon) + \sigma\nu_{81}(\varepsilon)$; from Hayashi (Ref. 40).

3.6.2. Vibrational Excitation

The CCl_2F_2 molecule has nine nondegenerate vibrational modes of which five ($\nu_1, \nu_2, \nu_4, \nu_6$, and ν_8) are infrared (IR) active (see Table 4). The Born dipole approximation for the total vibrational excitation cross section (the sum of the cross sections for $\nu_1, \nu_2, \nu_4, \nu_6$, and ν_8) has been calculated by Mann and Linder[19] and is shown in Fig. 9(a). This sum (Table 9) represents the total *direct* vibrational excitation cross section, $\sigma_{vib, dir, t}(\varepsilon)$, for this molecule.

Hayashi[40] obtained vibrational cross sections designated by him as $\sigma\nu_3$ and $\sigma\nu_{81}$ from a Boltzmann code analysis. The sum of these cross sections is compared in Fig. 9(b) with the $\sigma_{vib, dir, t}(\varepsilon)$ [Fig. 9(a)] and $\sigma_{sc, t}(\varepsilon) - \sigma_{e, int}(\varepsilon)$. The sum $\sigma\nu_3 + \sigma\nu_{81}$ of the Hayashi cross sections should contain both direct and indirect vibrational excitation and, thus, it should be larger than $\sigma_{vib, dir, t}(\varepsilon)$ but it should not exceed $\sigma_{sc, t}(\varepsilon) - \sigma_{e, int}(\varepsilon)$. The large difference between $\sigma\nu_3 + \sigma\nu_{81}$ and $\sigma_{sc, t}(\varepsilon) - \sigma_{e, int}(\varepsilon)$ indicates that the Hayashi cross sections are in error.

The excitation functions for some of the vibrational modes of CCl_2F_2 have been measured by Mann and Linder[19] and are shown in Fig. 10. Clearly, below 1 eV *direct* electron

TABLE 9. Total direct vibrational excitation cross section (Born dipole), $\sigma_{vib.\,dir.,f}(\varepsilon)$, for CCl_2F_2[a]

Energy (eV)	$\sigma_{vib.\,dir.,f}(\varepsilon)(10^{-20}\ m^2)$
0.03	0.20
0.035	0.25
0.04	0.30
0.045	0.34
0.05	0.38
0.06	0.43
0.07	0.48
0.08	0.52
0.09	0.61
0.10	0.88
0.125	3.92
0.15	7.59
0.20	10.93
0.25	11.06
0.30	10.61
0.35	10.03
0.40	9.48
0.45	8.91
0.50	8.39
0.60	7.53
0.70	6.83
0.80	6.29
0.90	5.78
1.0	5.39
1.5	4.05
2.0	3.23
2.5	2.73
3.0	2.38
3.5	2.08
4.0	1.84
5.0	1.48
6.0	1.27
7.0	1.09
8.0	0.94
9.0	0.85
10.0	0.80

[a]From Fig. 3 of Ref. 19.

scattering leads to strong excitation of the infrared active stretching modes. In the energy range between about 0.5 eV and 10 eV the predominant mode of vibrational excitation is *indirect* scattering through the decay of the negative ion resonances of CCl_2F_2 in this energy range (Table 5; Fig. 3). This has been demonstrated by Mann and Linder who measured differential cross sections for vibrational excitation of CCl_2F_2 in the energy range 0.5–10 eV (see below).

3.6.3. Indirect Excitation Via Negative Ion Resonances

Based on information provided by various techniques we can conclude (refer to earlier discussion in Sec. 2 and Fig. 3) that there exist at least five negative ion states of CCl_2F_2 below the electronic excitation threshold (at ~7 eV) of the molecule located at: +0.4 eV, −0.9 eV, −2.5 eV, −3.5 eV, and −6.2 eV. The calculations of Tossell[24] (see also Ref. 38) show profound changes between the geometries of CCl_2F_2 and $CCl_2F_2^-$. Based on these calculations and on the calculations by Burrow *et al.*[39] it would seem reasonable to ascribe the adiabatic value of the electron affinity [+0.4 eV (Refs. 21–23); +0.67 eV (Ref. 24)] and the vertical electron affinity at −0.9 eV to the same lowest negative ion state (this of course would indicate a large internuclear relaxation in $CCl_2F_2^-$; see Sec. 6). According to an *ab initio* self consistent field (SCF) calculation on the neutral molecule by Burrow *et al.*,[39] four valence-type resonances are expected below about 5 eV which can be ascribed, in increasing energetic order, to the unoccupied orbitals a_1 (C–Clσ^*), b_2 (C–Clσ^*), a_1 (C–Fσ^*), and b_1 (C–F σ^*). Burrow *et al.* have ascribed the resonances they detected in an electron

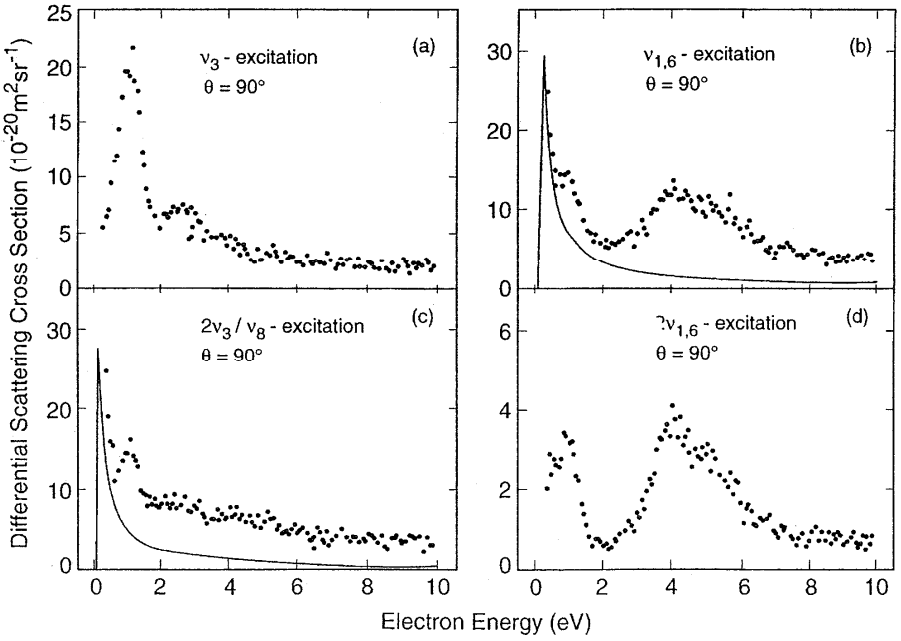

FIG. 10. Differential electron scattering cross sections as a function of electron energy for the most important energy-loss processes in electron-CCl_2F_2 collisions below 10 eV, at a scattering angle of 90°. The solid lines are the Born dipole cross sections for excitation of $\nu_{1,6}$, and ν_8 (from Mann and Linder, Ref. 19).

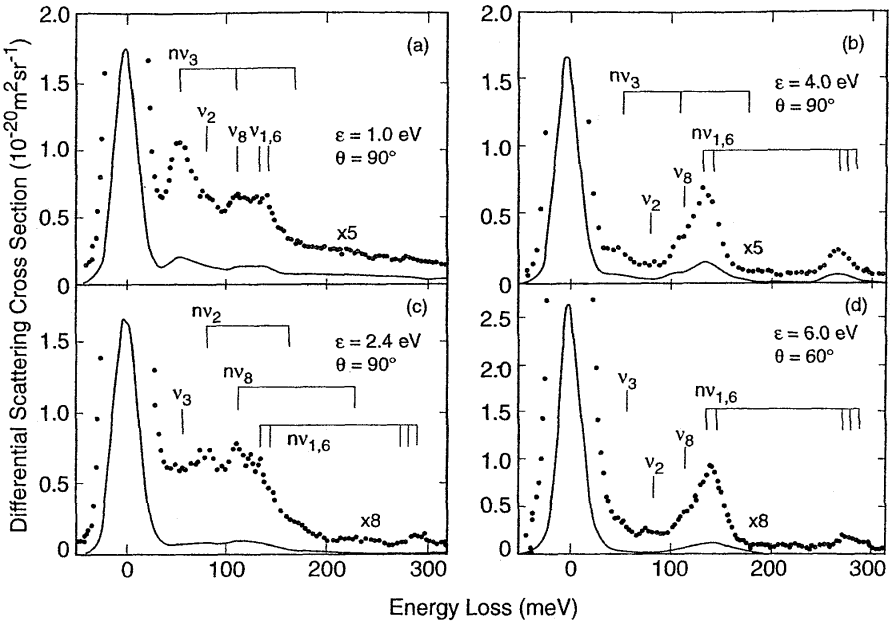

FIG. 11. Energy-loss spectra for electron-CCl_2F_2 scattering at scattering angles $\theta = 90°$ and 60° and incident electron energies of 1.0 eV, 2.4 eV, 4.0 eV, and 6.0 eV (from Mann and Linder, Ref. 19).

transmission experiment at 1 eV, 2.4 eV, and 3.9 eV to the lowest three of these molecular orbitals. With these findings in mind, Mann and Linder[19] measured the energy-loss spectra of CCl_2F_2 for electrons having initial energies equal to 1.0 eV, 2.4 eV, 4.0 eV, and 6.0 eV, i.e., roughly equal to the energy positions of the observed four resonances of CCl_2F_2. In Fig. 11 are shown their results. For 1.0 eV, the most prominent energy loss is assigned to the excitation of the ν_3 vibration. This is consistent with the (C–Clσ^*) character of the A_1 (C–Clσ^*) resonance at 1.0 eV. Also consistent with this assignment of the 1.0 eV resonance are the data on dissociative electron attachment around this energy (see Table 5), both for the production of Cl^- involving the C–Cl bond breaking and the production of Cl_2^- involving the C–Cl_2 dissociation. In vibrational excitation, the C–Cl_2 symmetric stretch mode ν_3 is the dominant excitation process.

Additionally, the data in Fig. 11 show that in the A_1(C–F σ^*) resonance at 4.0 eV, the excitation of $\nu_{1,6}$ is the dominating process. This is consistent with the (C–Fσ^*) character of this resonance. The A_1(C–Fσ^*) resonance at 4.0 eV is also the appropriate precursor of the group of the fragment negative ions observed at 3.5 eV (the position of the resonance apparently is shifted downward by about 0.5 eV in the dissociative attachment channel in comparison to the scattering channel). The dominant fragment anion at this energy is F^- and this is in accord with the (C–Fσ^*) character of this resonance.

With regard to the 2.5 eV resonance, it is clear that if the resonance assignments mentioned above are adopted, the B_2(C–Clσ^*) resonance at 2.5 eV does not seem to decay via dissociative attachment since none of the electron attachment studies have shown a peak at this energy. Peculiarly, the resonance shows up only in the vibrational excitation channel. Its energy-loss spectrum shows excitation of several modes none of which predominates [Fig. 11(c)].

Figure 12 shows the total indirect inelastic electron scattering cross section, $\sigma_{\text{inel, indir, t}}(\varepsilon)$, which we estimated by subtracting the sum $\sigma_{\text{vib, dir, t}}(\varepsilon) + \sigma_{\text{e, int}}(\varepsilon)$, as determined from Mann and Linder,[19] from our recommended values of $\sigma_{\text{sc, t}}(\varepsilon)$ (solid line, Fig. 4). The energy positions of the maxima in $\sigma_{\text{inel, indir, t}}(\varepsilon)$ are indicated in the figure by the vertical lines and are compared in Table 5 with other data. The maximum at 9.0 eV indicates the location of a negative ion state associated with the excited electronic states in this energy region.

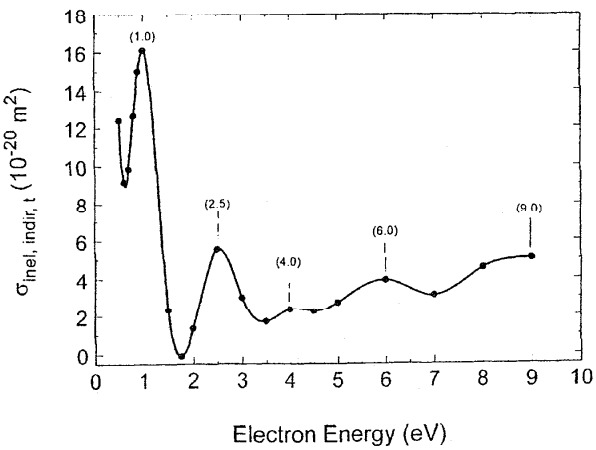

FIG. 12. Total indirect inelastic electron scattering cross section, $\sigma_{\text{in, indir, t}}(\varepsilon)$, as a function of electron energy for CCl_2F_2 (see text).

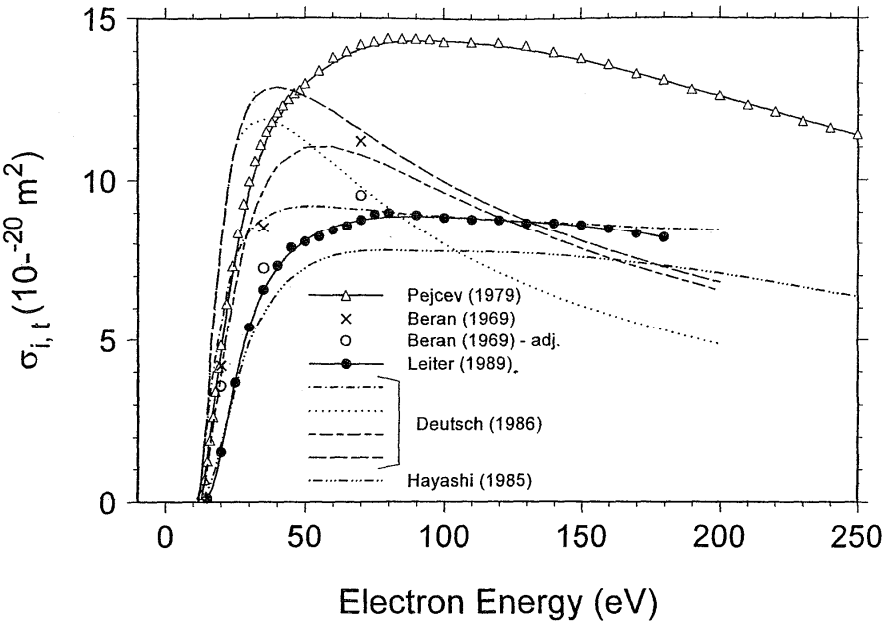

FIG. 13. Total ionization cross section, $\sigma_{i,t}(\varepsilon)$, as a function of electron energy for CCl_2F_2. Experimental data: △ (Ref. 31); ● (Ref. 49); × (Ref. 48); ○ (Ref. 48) adjusted (see text). Calculated data: (from Ref. 52); – – (Ref. 56); - — - (Ref. 55); ... (Ref. 54); – . – (Ref. 53); — ... — (Ref. 40).

It is thus seen (Figs. 10 and 11) that the $A_1(\text{C–Cl}\sigma^*)$ and $A_1(\text{C–F}\sigma^*)$ resonances are the dominant features in the vibrational excitation functions of the CCl_2F_2 molecule. As observed by Mann and Linder, the dominant vibrational excitation corresponds to the respective valence character of each resonance, i.e., ν_3 for the $A_1(\text{C–Cl}\sigma^*)$ resonance and ν_1 for the $A_1(\text{C–F}\sigma^*)$ resonance. The observed selective excitation of the CF_2 and CCl_2 stretching modes corresponding to the respective valence character of the resonance is in agreement with the symmetry selection rules.[19] The indirect excitation of the ν_1 and ν_3 vibrational modes is to be contrasted with the direct vibrational excitation of the infrared active modes $\nu_1, \nu_2, \nu_4, \nu_6$, and ν_8 at lower energies.

3.6.4. Electronic Excitation

The threshold for electronic excitation of the CCl_2F_2 is about 7.0 eV (Table 2) and the threshold for electron impact ionization is about 12.3 eV (Table 3). There are no data on the cross section for electronic excitation of CCl_2F_2. An estimate of the sum $\sigma_{\text{inel},t}(\varepsilon) + \sigma_{\text{e. int}}(\varepsilon)$ can be obtained from

$$\sigma_{\text{sc},t}(\varepsilon) - \sigma_{\text{i},t}(\varepsilon) - \sigma_{\text{a. diss},t}(\varepsilon) = \sigma_{\text{inel},t}(\varepsilon) + \sigma_{\text{e. int}}(\varepsilon), \quad (1)$$

and is discussed in Sec. 5.

4. Electron Impact Ionization

4.1. Total Ionization Cross Section, $\sigma_{i,t}(\varepsilon)$

There have been three experimental measurements[31,48,49] of the total ionization cross section of CCl_2F_2. The first measurements are those of Beran and Kevan[48] which were made for only three values of the incident electron energy. The second set of measurements is that of Pejčev *et al.*[31] who used a parallel plate condenser-type ionization chamber and a trochoidal electron monochromator as the electron source to cover the energy range from threshold to 250 eV. The third set of measurements is by Leiter *et al.*[49] who employed a double focusing sector field mass spectrometer. They reported absolute partial (see Sec. 4.2) ionization cross sections from threshold to 180 eV and determined the absolute total ionization cross section by taking the charge-weighted sum of their partial ionization cross sections. Leiter *et al.*[49] estimated the uncertainty of their total ionization cross section measurements to be ± 10%. No uncertainty values were stated by Pejčev *et al.*[31] The results of these three groups of investigators are shown in Fig. 13. There is substantial disagreement among these data. The values of Beran and Kevan[48] for a number of atomic and molecular species are consistently higher by about 15% compared to the more reliable measurements of Rapp and Englander-Golden.[50] We thus reduced the values of Beran and Kevan[48] by 15%. Their adjusted data are shown in Fig. 13 by the open circles and are seen to be in reasonable agreement with the measurements of Leiter *et al.*[49] The measurements of Pejčev *et al.*[31] although similar in shape to the data of Leiter *et al.*[49] are higher by as much as a factor of 2. Although the total ionization cross section values of Leiter *et al.* may be low due to the fact that their measurements have not been corrected for possible discrimination of the energetic fragment ions,[51] they are in better agreement with the corrected values of Beran and Kevan.[48] It should also be noted that since the predominant positive ion is $CClF_2^+$, the effects of ion discrimination on the value of the total ionization cross section may not be large.

TABLE 10. Recommended total ionization cross section, $\sigma_{i,t}(\varepsilon)$, for CCl_2F_2[a]

Electron energy (eV)	$\sigma_{i,t}(\varepsilon)(10^{-20}\ m^2)$
15	0.12
20	1.55
25	3.67
30	5.40
35	6.56
40	7.32
45	7.88
50	8.07
55	8.22
60	8.43
65	8.57
70	8.76
75	8.95
80	8.99
90	8.92
100	8.84
110	8.78
120	8.76
130	8.66
140	8.65
150	8.59
160	8.46
170	8.31
180	8.17

[a]Data of Leiter *et al.* (Ref. 49).

Also shown in Fig. 13 are the results of a number of calculations by Deutsch *et al.*[52] using empirically modified collision theories.[53–56] Interestingly, the calculations seem to be more consistent with the data of Pejčev *et al.*[31] below about 50 eV and with the data of Leiter *et al.*[49] at the higher energies. The total ionization cross section deduced by Hayashi[40] lies below all data, experimental and calculated. Clearly more measurements are indicated. Based primarily upon the apparent agreement between the measurements of Leiter *et al.* and the adjusted data of Beran and Kevan we tentatively suggest the data of Leiter *et al.* which are listed in Table 10.

4.2. Partial Ionization Cross Sections, $\sigma_{i,\,part}(\varepsilon)$

Leiter *et al.*[49] have measured absolute partial cross sections for the production of the following singly ionized species by electron impact on CCl_2F_2: $CCl_2F_2^+$, CCl_2F^+, $CClF_2^+$, CCl_2^+, Cl_2^+, $CClF^+$, ClF^+, CF_2^+, CCl^+, Cl^+, CF^+, F^+, and C^+. They reported an uncertainty in these values of about $\pm 10\%$.

These measurements are shown in Fig. 14 and are listed in Table 11. By far the largest cross section over the entire energy range covered is that for the $CClF_2^+$ positive ion. The cross section for this ion is about five times larger than the next most abundant ion, and is about 400 times larger than that for the parent positive ion $CCl_2F_2^+$. This clearly shows that for this molecule the preponderance of ionizing collisions are dissociative. The multiplicity of dissociation channels leads to a multiplicity of neutral and charged particles and demonstrates the extreme fragility of this molecule toward low energy electrons. The energy dependencies of the

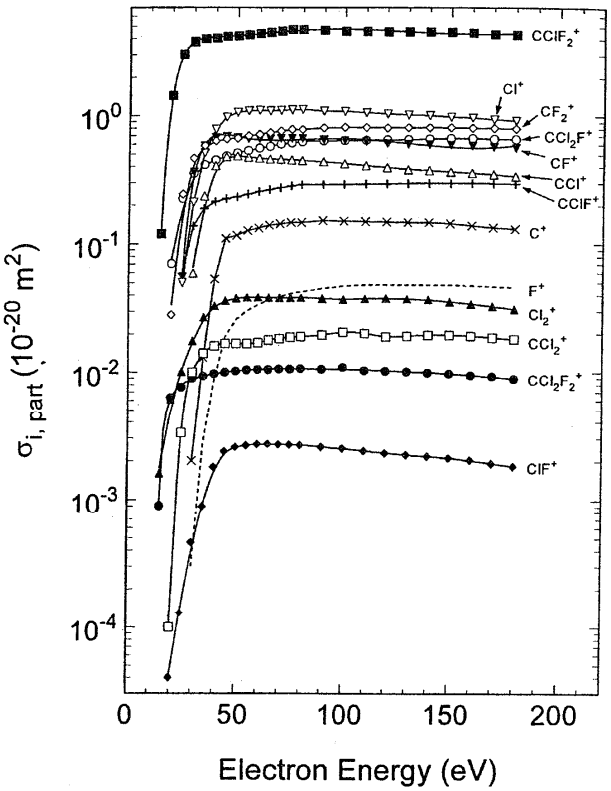

FIG. 14. Partial ionization cross sections, $\sigma_{i,\,part}(\varepsilon)$, as a function of electron energy for CCl_2F_2, in units of 10^{-20} m^2 (data of Leiter *et al.*, Ref. 49).

partial cross sections are rather similar, except when a number of different processes contribute to the formation of a particular positive ion which have different energetic onsets (e.g., Cl_2^+, CF_2^+, CCl_2^+, F^+, Cl^+). Leiter *et al.* reported no ionization threshold energies for these species. We have used their cross section data in Table 11 and estimated the energy thresholds for a number of singly charged positive ions which are listed in Table 12. In Table 12 are given also threshold energies for the production of singly positive ions via a number of photoprocesses. The electron impact values of the threshold energies for the various positive ions exceed the corresponding values obtained using photoionization methods, indicating differences in the adiabatic and vertical values of the thresholds.

From Fig. 14 one can easily find the relative abundance of the various positive ions from CCl_2F_2 at various incident electron energies (say, 70 eV).

4.3. Multiple (Double) Ionization Cross Sections, $\sigma_{i,\,mult}(\varepsilon)$

Cross sections for doubly charged positive ions produced in electron collisions with CCl_2F_2 have also been reported by Leiter *et al.*[49] These are listed in Table 13 and are plotted in Fig. 15. The reported uncertainty is $\pm 20\%$. The cross sections for doubly ionized species are generally much smaller compared to the cross sections for singly ionized species.

TABLE 11. Partial electron impact ionization cross sections, $\sigma_{i,part}(\varepsilon)$, in units of 10^{-20} m^2, for the production of singly ionized species from CCl_2F_2[a]

	Singly ionized species												
Energy (eV)	$CCl_2F_2^+$	CCl_2F^+	$CClF_2^+$	CCl_2^+	Cl_2^+	$CClF^+$	ClF^+	CF_2^+	CCl^+	Cl^+	CF^+	F^+	C^+
15	0.0009		0.12		0.0016								
20	0.0063	0.070	1.44	0.0001	0.0061		0.000 04	0.028					
25	0.0076	0.225	3.02	0.0033	0.0101	0.059	0.000 13	0.243		0.05	0.055		
30	0.0089	0.352	3.78	0.0100	0.0175	0.137	0.000 46	0.462	0.059	0.21	0.360	0.0003	0.002
35	0.0093	0.411	3.99	0.0140	0.0268	0.187	0.000 89	0.583	0.235	0.51	0.579	0.0027	0.013
40	0.0097	0.447	4.05	0.0160	0.0329	0.212	0.001 79	0.632	0.403	0.78	0.671	0.0087	0.053
45	0.0100	0.482	4.17	0.0167	0.0360	0.223	0.002 36	0.656	0.475	0.97	0.686	0.0189	0.110
50	0.0102	0.510	4.21	0.0167	0.0378	0.231	0.002 55	0.664	0.481	1.06	0.671	0.0257	0.116
55	0.0104	0.531	4.28	0.0167	0.0383	0.242	0.002 63	0.693	0.470	1.09	0.655	0.0301	0.126
60	0.0105	0.556	4.39	0.0170	0.0383	0.254	0.002 69	0.713	0.463	1.10	0.658	0.0336	0.132
65	0.0105	0.573	4.48	0.0178	0.0381	0.263	0.002 69	0.733	0.455	1.09	0.658	0.0366	0.139
70	0.0106	0.598	4.60	0.0183	0.0380	0.272	0.002 68	0.757	0.453	1.10	0.661	0.0388	0.142
75	0.0106	0.612	4.72	0.0188	0.0381	0.281	0.002 67	0.778	0.449	1.11	0.664	0.0410	0.146
80	0.0107	0.626	4.72	0.0190	0.0383	0.288	0.002 65	0.780	0.444	1.12	0.661	0.0424	0.146
90	0.0106	0.637	4.66	0.0196	0.0376	0.290	0.002 56	0.802	0.436	1.09	0.649	0.0451	0.151
100	0.0110	0.640	4.60	0.0206	0.0370	0.290	0.002 50	0.810	0.420	1.08	0.640	0.0470	0.150
110	0.0104	0.644	4.58	0.0202	0.0376	0.293	0.002 40	0.810	0.408	1.06	0.631	0.0481	0.149
120	0.0103	0.651	4.54	0.0191	0.0380	0.294	0.002 31	0.806	0.394	1.04	0.610	0.0484	0.148
130	0.0102	0.654	4.54	0.0193	0.0375	0.297	0.002 24	0.810	0.380	1.02	0.603	0.0481	0.147
140	0.0100	0.661	4.54	0.0196	0.0370	0.298	0.002 18	0.810	0.375	1.01	0.600	0.0481	0.147
150	0.0098	0.668	4.52	0.0196	0.0356	0.298	0.002 12	0.810	0.366	0.98	0.594	0.0481	0.144
160	0.0095	0.668	4.44	0.0193	0.0343	0.299	0.002 04	0.806	0.358	0.97	0.585	0.0475	0.139
170	0.0093	0.661	4.35	0.0187	0.0329	0.297	0.001 92	0.802	0.349	0.94	0.573	0.0467	0.134
180	0.0089	0.658	4.28	0.0182	0.0311	0.295	0.001 83	0.794	0.337	0.92	0.564	0.0459	0.131

[a]Data of Leiter *et al.* (see Ref. 49).

From the data of Leiter *et al.* we also estimated the energetic thresholds for doubly charged ions listed in Table 12 by a linear extrapolation of their cross sections to zero.

4.4. Ionization Coefficients

4.4.1. Density-Reduced Ionization Coefficient, α/N

There have been a number of measurements of the density-reduced ionization coefficient, α/N, which are compared in Fig. 16. The agreement is generally good except at low E/N. These measurements have generally been made at temperatures between 293 K and 295 K and have estimated uncertainties ranging from ±3% (Ref. 63), to ±5% (Ref. 64), to ±10% (Refs. 65–67). The solid curve in Fig. 16 is a least squares fit to the six sets of experimental data. Values for this curve are listed in Table 14 as our recommended data set for the α/N (E/N) of CCl_2F_2.

4.4.2. Average Energy to Produce an Electron-Ion Pair, W

The average energy to produce an electron-ion pair, W, by high-energy α particles slowed down in pure CCl_2F_2 is 29.5 eV.[70]

4.4.3. Gas Mixtures

Measurements have been reported also of the ionization coefficient (α/N) and effective ionization coefficient $[(\alpha-\eta)/N]$ of binary mixtures of CCl_2F_2 with a number of gases. Information on these can be found as follows:

$\alpha/N(E/N)$: CCl_2F_2/N_2 (Refs. 66 and 71–73); CCl_2F_2/air (Ref. 63); CCl_2F_2/SF_6 (Refs. 69 and 75); CCl_2F_2/CO_2 (Refs. 74 and 76); $(\alpha-\eta)/N(E/N)$: CCl_2F_2/N_2 (Refs. 67, 71, and 73); CCl_2F_2/SF_6 (Refs. 69 and 75); CCl_2F_2/CO_2 (Refs. 74 and 76).

5. Electron Impact Dissociation Producing Neutral Species

There have been no measurements of the total dissociation cross section for neutral species, $\sigma_{diss,\,neut,\,t}(\varepsilon)$, for this molecule. Based on the values of this cross section for CF_4 (Ref. 5) and CHF_3 (Ref. 43), the $\sigma_{diss,\,neut,\,t}(\varepsilon)$ for CCl_2F_2 is expected to be much smaller than the total scattering cross section $\sigma_{sc,\,t}(\varepsilon)$. It could, in principle, be determined from

$$\sigma_{diss,\,neut,\,t}(\varepsilon)=\sigma_{sc,\,t}(\varepsilon)-[\sigma_{e,\,int}(\varepsilon)+\sigma_{i,\,t}(\varepsilon)+\sigma_{vib,\,dir,\,t}(\varepsilon)+\sigma_{vib,\,indir,\,t}(\varepsilon)+\sigma_{a,\,t}(\varepsilon)+\sigma_{electronic,\,t}(\varepsilon)], \quad (2)$$

if all of the cross sections on the right-hand side of Eq. (2) were known. In Eq. (2), $\sigma_{electronic,\,t}(\varepsilon)$ represents the total cross section for electronic excitation not leading to dissociation or ionization and is expected to be small. In the present state of the available measurements, the only quantity one can derive with confidence from the above equation is the difference $\sigma_{sc,\,t}(\varepsilon)-\sigma_{i,\,t}(\varepsilon)$ which represents the nonionizing part of the total scattering cross section, $\sigma_{non\text{-}ionizing,\,t}(\varepsilon)$. This has been obtained for energies up to 200 eV, using the

TABLE 12. Threshold energies, in eV, for the production of positive ions by electron impact on CCl_2F_2[a]

Positive ion	Threshold energy (electron impact)[b] (eV)	Threshold energy (photophysical data for the indicated reaction or positive ion) (eV)	Positive ion	Threshold energy (electron impact)[b] (eV)	Threshold energy (photophysical data for the indicated reaction or positive ion) (eV)
$CCl_2F_2^+$	13.9	11.8 (Ref. 6)[d]	Cl^+	20.0	$Cl^+ + CF_2 + Cl$
	~12.3[c]	11.75 (Ref. 11)			18.5 (Ref. 6)[d]
		11.75 (Ref. 57)			18.76±0.05 (Ref. 62)
		11.87 (Ref. 58)			$Cl^+ + CF + FCl$
		12.24±0.01 (Ref. 59)			21.2 (Ref. 6)[d]
		12.26 (Ref. 60)			20±1 (Ref. 6)
		12.31±0.05 (Ref. 61)			$Cl^+ + CF + F + Cl$
					23.8 (Ref. 6)[d]
CCl_2F^+	17.9	14.0±1 (Ref. 6)			$Cl^+ + C + FCl + F$
		14.15 (Ref. 11)			26.8 (Ref. 6)[d]
		13.81 (Ref. 57)			$Cl^+ + C + F_2 + Cl$
		13.30±0.05 (Ref. 62)			27.7 (Ref. 6)[d]
					$Cl^+ + C + 2F + Cl$
$CClF_2^+$	15.1	11.5±1 (Ref. 6)			29.3 (Ref. 6)[d]
		12.10 (Ref. 11)			
		11.99 (Ref. 57)	F^+	30.0	$F^+ + CF + Cl_2$
		11.96±0.3 (Ref. 62)			25.7 (Ref. 6)[d]
					$F^+ + CF + 2Cl$
CCl_2^+	21.7	46±1 (Ref. 6)			28.2 (Ref. 6)[d]
					$F^+ + C + FCl + Cl$
CF_2^+	19.1	$CF_2^+ + Cl_2$			31.2 (Ref. 6)[d]
		14.6 (Ref. 6)[d]			$F^+ + C + F + Cl_2$
		14.90±0.3 (Ref. 62)			31.3 (Ref. 6)[d]
		$CF_2^+ + 2Cl$			$F^+ + C + F + 2Cl$
		17.1 (Ref. 6)[d]			33.8 (Ref. 6)[d]
		17.5±1 (Ref. 6)			36±1 (Ref. 6)
		17.22 (Ref. 11)			
		16.98 (Ref. 57)	C^+	31.8	$C^+ + 2FCl$
					20.5 (Ref. 6)[d]
$CClF^+$	21.7	18.5±1 (Ref. 6)			$C^+ + F_2 + Cl_2$
		17.76 (Ref. 57)			23.5 (Ref. 6)[d]
		18.60±0.05 (Ref. 62)			$C^+ + FCl + F + Cl$
					25.1 (Ref. 6)[d]
Cl_2^+	12.2	$Cl_2^+ + CF_2$			$C^+ + 2F + Cl_2$
		15.40±0.1 (Ref. 62)			25.1 (Ref. 6)[d]
					$C^+ + F_2 + 2Cl$
ClF^+	18.3				26.0 (Ref. 6)[d]
					$C^+ + 2F + 2Cl$
CCl^+	27.3	24±1 (Ref. 6)			27.6 (Ref. 6)[d]
		21.60±0.1 (Ref. 62)			31±1 (Ref. 6)
CF^+	23.0	$CF^+ + F + Cl_2$	Cl^{++}	52.2	
		17.4 (Ref. 6)[d]			
		17.65 (Ref. 11)	CCl^{++}	48.7	
		17.35±0.05 (Ref. 62)			
		$CF^+ + F + 2Cl$	CCl_2^{++}	40.0	
		19.9 (Ref. 6)[d]			
		20±1 (Ref. 6)	$CClF^{++}$	40.0	
		20.20 (Ref. 11)			
		19.84±0.05 (Ref. 62)	$CClF_2^{++}$	37.9	38±1 (Ref. 6)
		$CF^+ + FCl + Cl$			
		17.3 (Ref. 6)[d]	CCl_2F^{++}	33.9	

[a]Photophysical data are also listed for comparison when available.
[b]Present estimates based on the data of Leiter *et al.* (Ref. 49). These estimates are very approximate and are intended to be used for guiding purposes only.
[c]From Table 3 of this article.
[d]Calculated by Zhang *et al.* (Ref. 6) using thermochemical data under the assumption of zero kinetic energy of fragmentation.

TABLE 13. Multiple (double) ionization cross sections, $\sigma_{i,\,mult}(\varepsilon)$, in units of 10^{-22} m^2, in electron collisions with CCl_2F_2[a]

Energy (eV)	Cl^{++}	CCl^{++}	CCl_2^{++}	$CClF^{++}$	$CClF_2^{++}$	CCl_2F^{++}
40			0.06	0.004	0.09	0.34
45			0.45	0.052	0.39	0.99
50			1.07	0.104	0.71	1.50
55	0.006	0.15	1.52	0.221	1.00	1.88
60	0.019	0.31	1.88	0.274	1.23	2.10
65	0.048	0.54	2.08	0.321	1.39	2.29
70	0.091	0.66	2.25	0.358	1.51	2.44
75	0.134	0.74	2.37	0.388	1.60	2.58
80	0.164	0.81	2.46	0.408	1.67	2.66
90	0.215	0.91	2.61	0.443	1.76	2.82
100	0.250	0.99	2.70	0.470	1.80	2.90
110	0.272	1.02	2.78	0.487	1.82	2.93
120	0.287	1.03	2.81	0.497	1.80	2.92
130	0.294	1.03	2.83	0.499	1.78	2.90
140	0.296	1.04	2.79	0.497	1.76	2.88
150	0.293	1.03	2.77	0.492	1.72	2.85
160	0.287	1.02	2.74	0.485	1.69	2.78
170	0.279	0.99	2.68	0.473	1.65	2.71
180	0.272	0.98	2.62	0.460	1.60	2.64

[a]Data of Leiter *et al.* (See Ref. 49.)

average value of $\sigma_{sc,\,t}(\varepsilon)$ in Fig. 4 and the data of Leiter *et al.*[49] for $\sigma_{i,\,t}(\varepsilon)$, and is shown in Fig. 17. Above 10 eV the cross sections for direct and indirect vibrational excitation and electron attachment are small, so in this energy range Eq. (2) may be written as

$$\sigma_{sc,\,t}(\varepsilon)-\sigma_{i,\,t}(\varepsilon)\simeq\sigma_{e,\,int}(\varepsilon)+\sigma_{diss,\,neut,\,t}(\varepsilon)+\sigma_{electronic,\,t}(\varepsilon). \quad (3)$$

Since, moreover, electronic excitation predominantly leads to dissociation and the cross section for dissociation into neutral species is expected[5,43] to be small compared to $\sigma_{sc,\,t}(\varepsilon)$ and $\sigma_{i,\,t}(\varepsilon)$, Eq. (3) may be further reduced to

$$\sigma_{sc,\,t}(\varepsilon)-\sigma_{i,\,t}(\varepsilon)\simeq\sigma_{e,\,int}(\varepsilon). \quad (4)$$

Unfortunately $\sigma_{e,\,int}(\varepsilon)$ is only known for energies $\leq$ 10 eV. Above this energy Eq. (4) can only give an upper limit for $\sigma_{e,\,int}(\varepsilon)$. This relationship seems to be consistent with the existing measurements as can be seen from Fig. 17.

6. Electron Attachment

There have been numerous measurements of electron attachment coefficients in CCl_2F_2. We begin this section by analyzing these measurements because they provide an insight for understanding the electron attachment cross section data which are presented later in the article (Sec. 6.5).

6.1. Density-Reduced Electron Attachment Coefficient, η/N

The density-reduced electron attachment coefficient, η/N, of CCl_2F_2 has been measured as a function of E/N both in the pure gas and in mixtures of CCl_2F_2 with a number of gases. The quantity $\eta/N(E/N)$ is related to the total electron attachment cross section, $\sigma_{a,\,t}(\varepsilon)$, and the electron energy distribution function $f(\varepsilon,E/N)$ in the gas/gas mixture by

$$\eta/N_a(E/N)=(2/m)^{1/2}w^{-1}\int_0^\infty f(\varepsilon,E/N)\varepsilon^{1/2}\sigma_{a,\,t}(\varepsilon)d\varepsilon, \quad (5)$$

where N_a is the number density of the electron attaching gas and w is the electron drift velocity. For the unitary gas, the total number density $N=N_a$; for its mixtures in a buffer gas of density N, N_a is much less than N.

The density-normalized electron attachment coefficient of CCl_2F_2 has been measured by a number of investigators.[63–69,71,72] Figure 18 shows these measurements which were made at temperatures ranging from 293 K to 298 K. The quoted uncertainties vary from ±5% to ±15% [±5% (Ref. 64), ±15% (Ref. 63), ±10% (Ref. 65), ±10% (Ref. 66)]. With the exception of the data of Siddagangappa *et al.*[71] and Harrison and Geballe,[68] there is reasonable agreement among the measurements. The solid line in Fig. 18 represents the least squares fitting average of all the data except those of Refs. 68 and 71. Values from the solid line are given in Table 15, and are our recommended values.

6.2. Total Electron Attachment Rate Constant, $k_{a,\,t}$

The density-reduced electron attachment coefficient $\eta/N_a(E/N)$ is related to the total electron attachment rate constant by

$$k_{a,\,t}(E/N)=\eta/N_a(E/N)\times w(E/N). \quad (6)$$

There have been four sets of measurements[26,27,29,30] of the $k_{a,\,t}(E/N)$ of CCl_2F_2 in N_2 buffer gas and one measurement[29] using Ar as the buffer gas. The variation of the $k_{a,\,t}$ of CCl_2F_2 with E/N measured in the buffer gases N_2 and Ar is shown in Fig. 19. There is a reasonable agreement for the measurements in N_2 whose uncertainties are all approximately ±10%.

The data in Fig. 19 and those of Christophorou *et al.*[26] are plotted in Fig. 20 as a function of the mean electron energy, $\langle\varepsilon\rangle$, determined from the buffer gas electron energy distribution functions. The data of Christophorou *et al.*[26] lie higher than the rest of the measurements and for this reason they were excluded from the averaging (Fig. 21). The average of all three sets of data in Fig. 21 is shown by the broken curve. In the averaging process the first two data points of McCorkle *et al.* were excluded, since none of the other three sets of similar measurements showed a downward trend. In Fig. 21 are also plotted the results of a number of studies which measured only the thermal ($T=300$ K) value of $k_{a,\,t}$. The average of all the values of $k_{a,\,t}$ at thermal energies is shown by ⊗.

Finally, there has been one other study[86] that reported electron attachment rate constants versus mean electron energy for CCl_2F_2 measured in mixtures with N_2. The energy dependence and the magnitude of the results of this study are at variance with the rest of the data in Fig. 21 and for this reason these data are not shown in the figure.

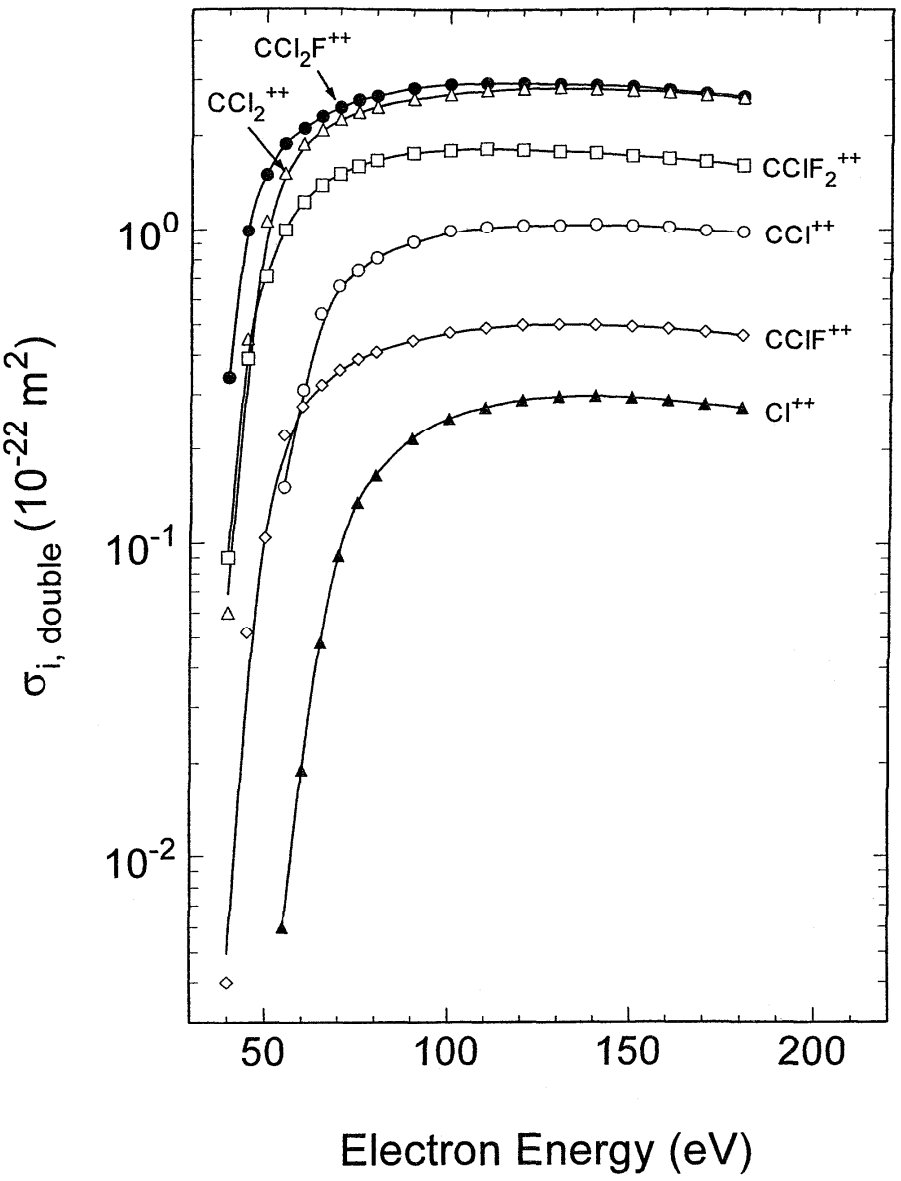

FIG. 15. Double ionization cross section, $\sigma_{i,\,double}(\varepsilon)$, in units of 10^{-22} m^2, for CCl_2F_2 (data of Leiter *et al.*, Ref. 49).

The average rate constant in Fig. 21 is compared in Fig. 22 with the data of Wang and Lee[29] in argon. The low-energy range data obtained from mixtures with N_2 and the high-energy range data obtained from measurements in mixtures with Ar merge smoothly to cover the energy range from 0.04 eV to 5 eV. Data taken off this figure are listed in Table 16 and represent our recommended set of values for the $k_{a,t}(\langle\varepsilon\rangle)$ of CCl_2F_2.

6.3. Thermal Value of the Total Electron Attachment Rate Constant, $(k_{a,t})_{th}$

The value of $k_{a,t}(E/N)$, when the electron energy distribution function $f(\varepsilon,E/N)$ is Maxwellian, $f_M(\varepsilon,T)$, i.e., when $E/N\rightarrow 0$, and $f(\varepsilon.E/N)$ is characteristic of only the gas temperature T, is referred to as the total thermal electron attachment rate constant $(k_{a,t})_{th}$ and is given by

$$(k_{a,t})_{th}=(2/m)^{1/2}w^{-1}\int_0^\infty f_M(\varepsilon,T)\varepsilon^{1/2}\sigma_{a,t}(\varepsilon)d\varepsilon. \quad (7)$$

Table 17 lists reported values of $(k_{a,t})_{th}$ measured at $T=293$–300 K. The mean of these values is $(15.5\pm7.5)\times10^{-10}$ cm^3 s^{-1}. These values have also been plotted in Fig. 21.

6.4. Effect of Temperature on $k_{a,t}$(E/N)

The data presented in Figs. 18–22 clearly show that the CCl_2F_2 molecule attaches electrons with energies down to 0

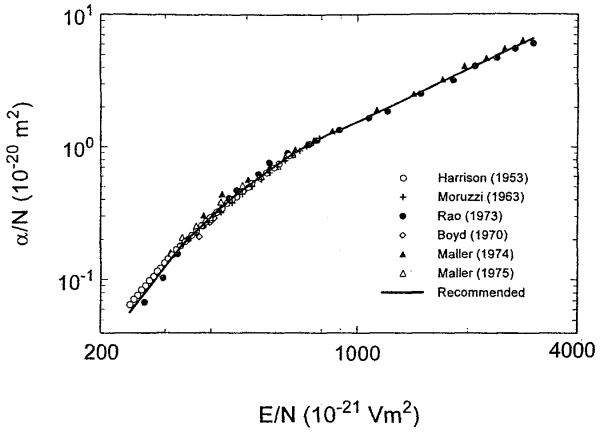

FIG. 16. Density-reduced ionization coefficient, $\alpha/N(E/N)$, for CCl_2F_2, in units of 10^{-20} m^2. ○ (Ref. 68); + (Ref. 64); ● (Ref. 63); ◇ (Ref. 65); ▲ (Ref. 67); △ (Ref. 66); — (recommended).

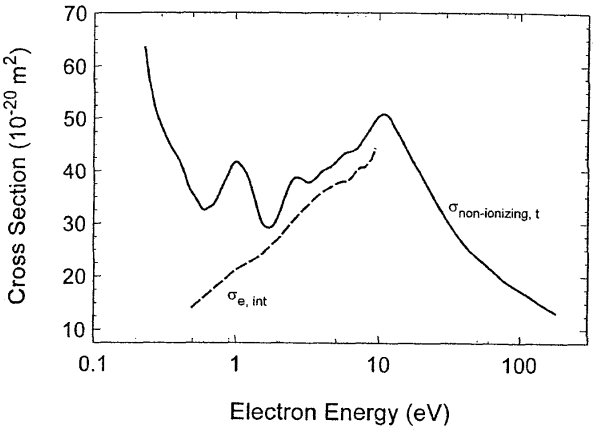

FIG. 17. Nonionizing part, $\sigma_{\text{non-ionizing},t}(\varepsilon)$, of the total electron scattering cross section for CCl_2F_2.

eV. Furthermore, the data on electron attachment and electron scattering in Sec. 3 show that the lowest vertical attachment energy of CCl_2F_2 is -0.9 eV and its adiabatic electron affinity $+0.4$ eV. The latter finding suggests that the potential energy surface of the lowest negative ion state of CCl_2F_2 has a minimum about 0.4 eV below that of the neutral molecule. It is possible (see Fig. 23) that the potential energy surface of this state rises steeply in the Franck–Condon region to account for the lowest vertical attachment energy of -0.9 eV. The preponderance of electron attachment reactions below about 1 eV (see next section) lead to dissociation of $CCl_2F_2^{-*}$ producing Cl^-. Since the CF_2Cl–Cl bond dissociation energy [3.3±0.2 eV (Ref. 21); 3.58 eV (Ref. 32); 3.1 eV (Ref. 87)] is smaller than the electron affinity (3.61 eV, Ref. 88) of the Cl atom, the reaction

TABLE 14. Recommended ionization coefficients, α/N, for CCl_2F_2

$E/N(10^{-21}$ V m$^2)$	$\alpha/N(10^{-20}$ m$^2)$
250	0.066
300	0.13
350	0.21
400	0.29
450	0.40
500	0.50
550	0.61
600	0.73
650	0.84
700	0.96
750	1.07
800	1.18
850	1.27
900	1.36
950	1.46
1000	1.56
1250	2.08
1500	2.65
2000	3.85
2500	5.15
3000	6.51

$$CCl_2F_2 + e \rightarrow CF_2Cl + Cl^- \quad (8)$$

is exoergic by ~ 0.28 eV.

The energy position of this (lowest) negative ion state would make the dissociative attachment process (8) highly temperature dependent (see, for example, Refs. 89–92) and hence, the rate constant would be expected to increase with increasing gas temperature. Indeed this has been shown to be the case both for the thermal value, $(k_{a,t})_{th}$, of $k_{a,t}$ (Refs. 30, 87, 93) and for the values of $k_{a,t}$ over a wider electron energy range (Ref. 30). In Table 18 measurements are listed of $(k_{a,t})_{th}$ at temperatures ranging from 205 K to 777 K. In order to discern the temperature variation of $(k_{a,t})_{th}$ these data are normalized to the average value of $(k_{a,t})_{th}$ at ~ 300 K (see Table 17) and are plotted in Fig. 24. Over this temperature range $(k_{a,t})_{th}$ increases by more than a factor of 300. The temperature enhancement of the electron attachment rate constant for mean electron energies to ~ 1.0 eV is shown in Fig. 25. These measurements are consistent with the results of a recent crossed beam study[94] shown in Fig. 26. These data are for the production of Cl^- from CCl_2F_2 and were taken with an electron energy resolution of ~ 60 meV. The observed pronounced enhancement suggests that dissociative electron attachment to hot CCl_2F_2 molecules is an effective way to decompose the CCl_2F_2 molecules. In contrast to these generally accepted data, one study[35] showed the rather peculiar behavior of the total electron attachment cross section at 563 K being lower than at 393 K. This is not understood.

6.5. Total Electron Attachment Cross Section, $\sigma_{a,t}(\varepsilon)$

There are three sources of total electron attachment cross sections for CCl_2F_2:

(i) swarm-unfolded cross sections using electron attachment rate constants measured in mixtures of CCl_2F_2 with N_2 (Refs. 26, 27, and 30) and in mixtures with N_2 and with Ar (Ref. 28 using the data of Ref. 29);

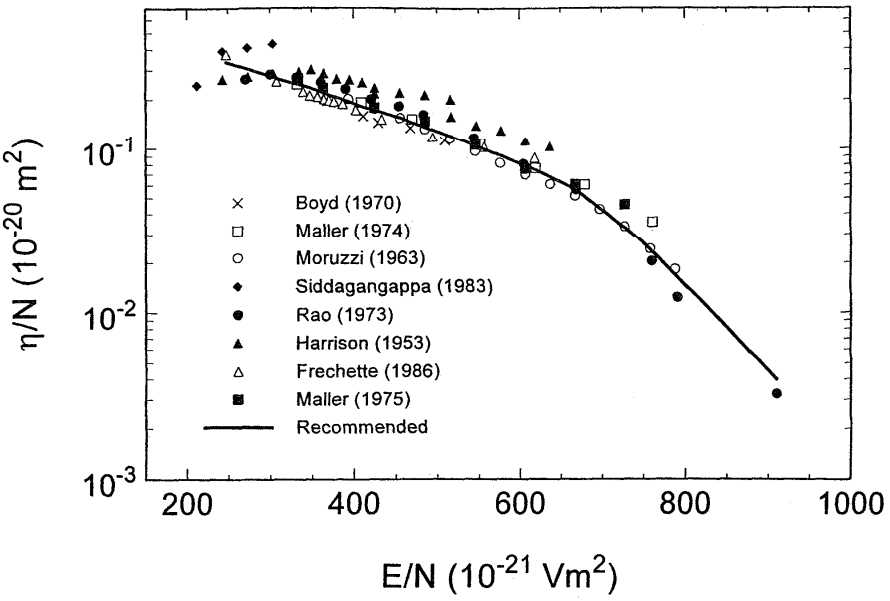

FIG. 18. Density-normalized electron attachment coefficient, $\eta/N(E/N)$, in units of 10^{-20} m^2, for CCl_2F_2. × (Ref. 65); □ (Ref. 67); ○ (Ref. 64); ◆ (Ref. 71); ● (Ref. 63); ▲ (Ref. 68); △ (Ref. 69); ■ (Ref. 66); — (recommended).

(ii) electron beam measurements using quasi-monoenergetic electrons;[31,35,93] and

(iii) threshold electron attachment using very-low-energy electrons produced by photoionization.[25]

The results of these methods are compared in Fig. 27 up to 5 eV. There is a considerable variation in these data. With the exception of the data of McCorkle *et al.*[27] and Illenberger *et al.*[32–34] which show a downward trend at the extreme low-energy range, the rest of the measurements show a steep increase in the attachment cross section as the electron energy approaches zero, including the very-low-energy data of Chutjian and Alajajian.[25] Moreover, recent measurements on Cl^- from CCl_2F_2 by Kiendler *et al.*[94] using a crossed beam experiment with a 60 meV energy resolution gave a cross section which rises steeply as the energy decreases in the extreme low-energy range in agreement with the rest of the data. We thus believe that the cross section rises as the energy decreases toward zero. Additionally, all data show a cross section maximum near 0.9 eV and the beam data of Pejčev *et al.*[31] and Underwood-Lemons *et al.*[35] also show a maximum at ~3.5 eV. We can therefore conclude that the electron attachment data indicate three negative ion states of CCl_2F_2 below ~4 eV at ≤0.0 eV, 0.9 eV, and 3.5 eV. This conclusion, as discussed in Section 2 (see Fig. 3), is consistent with the electron scattering data. Two swarm-unfolded cross sections[26,27] and one beam total electron attachment study[31] indicate structure at about 0.25 eV. Since no negative

TABLE 15. Density-normalized electron attachment coefficient, η/N_a, for CCl_2F_2 as a function of E/N

E/N(10^{-21} V m^2)	η/N_a(10^{-20} m^2)
250	0.33
300	0.27
350	0.23
400	0.19
450	0.16
500	0.13
550	0.10
600	0.082
650	0.062
700	0.042
750	0.026
800	0.015
850	0.008
900	0.005

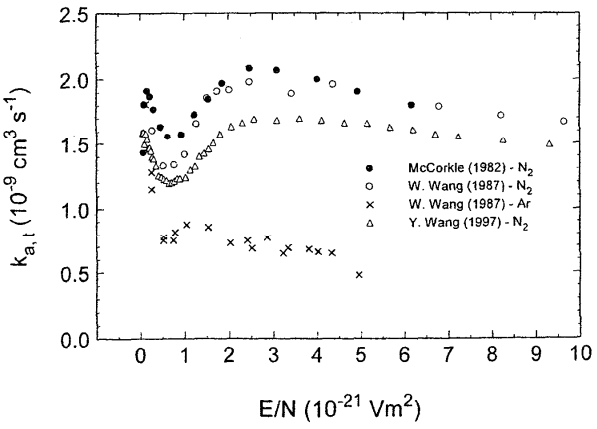

FIG. 19. Total electron attachment rate constant $k_{a,t}$ as a function of E/N for CCl_2F_2 measured in mixtures with N_2. ● (Ref. 27); ○ (Ref. 29); △ (Ref. 30), and Ar (x, Ref. 29).

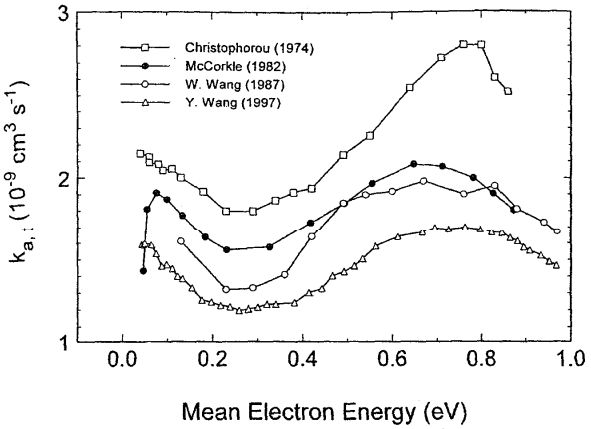

FIG. 20. Total electron attachment rate constant $k_{a,t}$ for CCl_2F_2 as a function of the mean electron energy, $\langle\varepsilon\rangle$, measured in a buffer gas of N_2. ● (Ref. 27); □ (Ref. 26); ○ (Ref. 29), △ (Ref. 30).

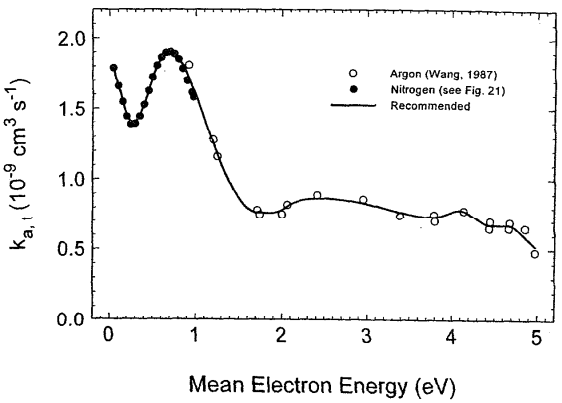

FIG. 22. Total electron attachment rate constant as a function of the mean electron energy, $k_{a,t}(\langle\varepsilon\rangle)$, for CCl_2F_2 measured in mixtures with N_2 and Ar. ● (average of the data in N_2 from Fig. 21). ○ (data of Ref. 29 for Ar mixtures). The solid line through the data points is a least squares fit to the data.

ion state is expected in this energy range, this possible structure may arise from dissociative electron attachment from vibrationally excited CCl_2F_2 molecules.

We have attempted to deduce recommended values of the total electron attachment cross section by a least squares fitting to the various data in Fig. 27 in the range of energies where they are most reliable.

Below 0.1 eV: In this energy range only the electron swarm[26,27,30] and the threshold electron attachment[25] data were used to obtain the average cross section because the electron beam measurements are known to be uncertain in this extreme low-energy range. In the averaging we excluded the lowest three points of the unfolded cross section given in Table V of McCorkle *et al.*[27] because in this energy range all other cross sections increase rather than decrease with decreasing electron energy. We also multiplied the cross section of Christophorou *et al.*[26] by 0.7 since their electron attachment rate constants had to be multiplied by this factor to be brought into agreement with other data of this type.

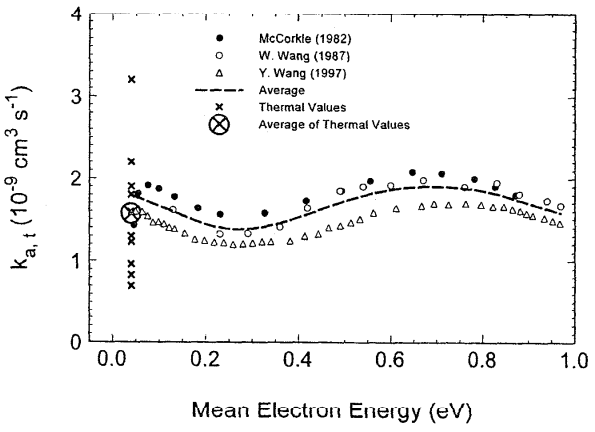

FIG. 21. Total electron attachment rate constant $k_{a,t}$ for CCl_2F_2 as a function of the mean electron energy, $\langle\varepsilon\rangle$, measured in a buffer gas of N_2. Also plotted are thermal values of $k_{a,t}$. ● (Ref. 27); ○ (Ref. 29), △ (Ref. 30). - - - (least squares average of all the data). × [thermal values of $k_{a,t}$ as measured by various groups using a number of techniques (Table 17)]. ⊗ (average of the thermal values of $k_{a,t}$).

Between 0.1 eV and 1.2 eV: In this energy range all data were used except we excluded from the averaging the normalized cross section of Illenberger *et al.*[32–34] on three grounds. First, the accuracy of the relative yields for the various negative ion fragments, especially at low electron energies, is uncertain as the authors themselves stated in their article. Second, below about 0.3 eV, the data of Illenberger *et al.* show the total electron attachment cross section decreasing precipitously with decreasing electron energy, in contrast to the most reliable beam and swarm data which show that the total electron attachment cross section rises steeply as the electron energy decreases toward zero. Third, the data are not absolute.

Energy >1.2 *eV*: In this energy range the accuracy of the beam data is superior to the swarm-unfolded cross sections (the latter[28] might also be influenced by the effect of the attaching gas on the distribution functions in pure argon used in the unfolding) and for this reason we averaged only the cross sections of the two electron beam studies, namely, those of Pejčev *et al.*[31] and Underwood-Lemons *et al.*[35]

The cross sections for the data used in each of the three energy regions, as discussed above, are plotted in Fig. 28 as a log-log plot, and the solid line in the figure is a least square fit to the measurements. Values taken off the smooth curve are listed in Table 19, and are our designated recommended values. The cross section deduced by Hayashi[40] is shown for reference, and is clearly in error. In Fig. 28 is also plotted the cross section for Cl^- from CCl_2F_2 measured recently by Kiendler *et al.*[94] using a crossed beam experiment. This cross section agrees with the rest of the data in the extreme low-energy range, but it progressively falls below the rest of the data; at ~1 eV where all the data are virtually in agreement, the cross section of Kiendler *et al.* is clearly much smaller.

TABLE 16. Recommended total electron attachment rate constant as a function of mean electron energy, $k_{a,t}(\langle\varepsilon\rangle)$, for CCl_2F_2

Mean electron energy (eV)	$k_{a,t}(\langle\varepsilon\rangle)(10^{-9}$ cm^3 s^{-1})
0.05	1.77
0.06	1.75
0.07	1.73
0.08	1.71
0.09	1.68
0.10	1.66
0.20	1.44
0.30	1.39
0.40	1.53
0.50	1.72
0.60	1.86
0.65	1.90
0.70	1.90
0.75	1.89
0.80	1.85
0.90	1.75
1.00	1.59
1.10	1.42
1.20	1.26
1.30	1.10
1.40	0.97
1.50	0.86
1.60	0.79
1.70	0.77
1.80	0.76
2.00	0.79
2.20	0.85
2.40	0.87
2.60	0.86
2.80	0.85
3.00	0.83
3.20	0.80
3.40	0.77
3.60	0.75
3.80	0.74
4.00	0.77
4.20	0.76
4.40	0.68
4.60	0.67
4.80	0.62
5.00	0.50

6.6. Dissociative-Electron-Attachment Fragment Anions

A number of electron beam studies[32–34,36,93,95,96] reported relative yields of fragment negative ions by electron impact on CCl_2F_2 as a function of electron energy (see also Table 5). Rosenbaum and Neuert[95] detected Cl^- and F^- with maximum intensities at 1.7 eV and 3.7 eV, respectively, Hickam and Berg[96] observed Cl^- with an appearance onset of 0.5 eV, and Verhaart *et al.*[36] found the yields of Cl^-, F^-, and CCl_2F^- to maximize, respectively, at 0.7 eV, 3.2 eV, and 3.7 eV. In another study, Chen and Chantry[93] found that the yield of Cl^- from CCl_2F_2 peaked at "very-near-zero energy" with a cross section at this energy of $\sim 5.4\times 10^{-16}$ cm^2. They also found that at temperatures above 500 K the production of Cl_2^- from CCl_2F_2 exhibits a small zero-energy peak which increases rapidly with increasing temperature.

TABLE 17. Thermal values, $(k_{a,t})_{th}$, of the total electron attachment rate constant[a] for CCl_2F_2

$(k_{a,t})_{th}(10^{-10}$ cm^3 s^{-1})	T (K)	Method	Reference
13.8	295	Electron swarm	30
9.6	295?	Electron swarm	77
13	298	Microwave conductivity	78
8.3	300	Electron cyclotron resonance	79
7	298	Electron cyclotron resonance	80
18	293	Electron cyclotron resonance	81
19	298	Electron swarm	82
12.3	298	Electron swarm	27,83
22	298	Electron swarm	26
32	300	Flowing afterglow	84,85

[a]Average value $(15.5\pm 7.5)\times 10^{-10}$ cm^3 s^{-1}.

Illenberger and co-workers[32–34] carried out the most comprehensive investigation of the relative intensities of the various fragment anions generated by electron impact on CCl_2F_2 as a function of electron impact energy. They measured the en-

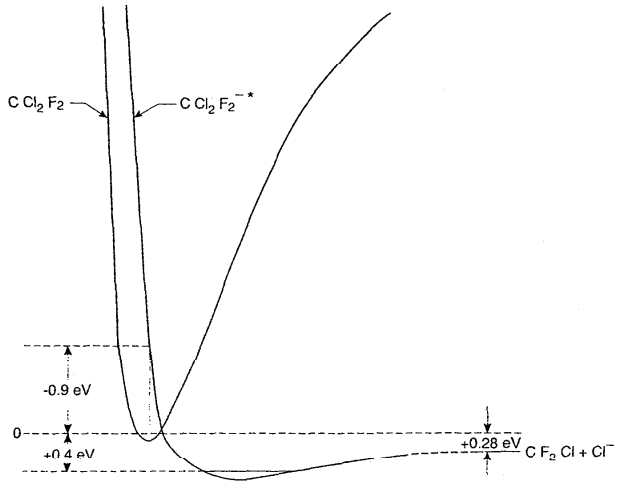

FIG. 23. Schematic potential energy curves for CF_2Cl–Cl and for the lowest negative ion state of $CCl_2F_2^-$* consistent with the (adiabatic) positive (+0.4 eV) electron affinity of CCl_2F_2, the vertical electron affinity (−0.9 eV) of the lowest negative ion state of CCl_2F_2, and the observation (see next section) that the dissociative electron attachment cross section rises steeply as the electron energy decreases towards zero. The asymptotic limit CF_2Cl + Cl^- lies 0.28 eV below the 0.0 eV level taken to be at the v=0 level of the CF_2Cl–Cl symmetric stretch vibration ν_3, using a value of 3.33 eV for the CF_2Cl–Cl dissociation energy and 3.61 eV for the electron affinity of the Cl atom (see text).

TABLE 18. $(k_{a,t})_{th}$ of CCl_2F_2 as a function of gas temperature

$(k_{a,t})_{th}(10^{-10}$ cm^3 s$^{-1})$	T (K)	Reference
<10	205	84, 85
32	300	
160	455	
530	590	
13.8	300	30
60	400	
<140	500	
19	293	92
140	467	
240	579	
420	777	

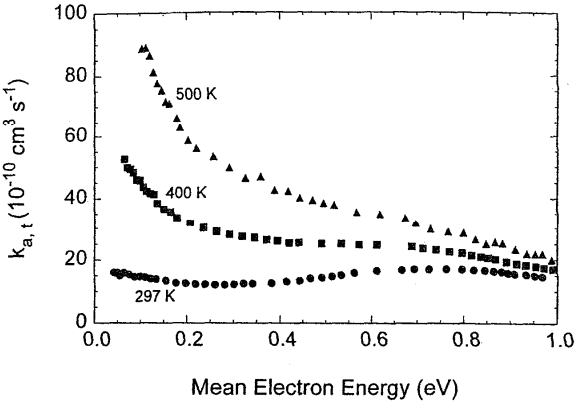

FIG. 25. Variation of $k_{a,t}(\langle\varepsilon\rangle)$ of CCl_2F_2 with temperature (Ref. 30).

ergy dependence of the intensities of the fragment anions F^-, Cl^-, ClF^-, Cl_2^-, and CCl_2F^- and reported approximate values of their relative energy-integrated intensities. We have multiplied the relative intensities of the various fragment anions reported by Illenberger and co-workers by the corresponding values of the energy-integrated intensities of the negative ions as given by Illenberger *et al.*[32] and the resultant relative cross sections are shown in Fig. 29. Clearly the resonance below 1 eV is predominantly due to Cl^- with some contribution from the Cl_2^- fragment. Many fragment anions contribute to the second broad maximum at ~3.5 eV, foremost F^-. These fragmentations are consistent with the symmetry of the negative ion states for the resonances at these energies as we have discussed earlier in the article.

We have taken the sum of the relative cross sections in Fig. 29 which is shown by the solid line in the figure. This sum was also plotted in Fig. 27 after it was normalized to the cross section of Pejčev *et al.*[31] at 0.7 eV. Clearly the shape of Illenberger's total cross section is not consistent with the rest of the data especially below ~0.5 eV, but these data still provide useful information concerning relative yields of negative ions.

6.7. Negative Ions in CCl_2F_2 Discharges

A number of studies have been conducted which utilize negative ions produced by dissociative electron attachment to CCl_2F_2 to study radio frequency (rf) discharges of this gas. Many of these studies dealt with the measurement of negative ion densities in rf discharges using a combination of microwave resonance and photodetachment techniques. As expected, these studies have found that Cl^- is the dominant fragment negative ion.[97] Askaryan *et al.*[98] found that "the mechanism of dissociative electron attachment which is manifested in a cold decaying plasma of a pulsed microwave discharge is a principal mechanism causing dissociation of chlorofluorocarbons (CCl_2F_2)." In another study involving negative ions of CCl_2F_2, the role of negative ions in particle formation in low-pressure discharges of the CCl_2F_2/Ar/Si

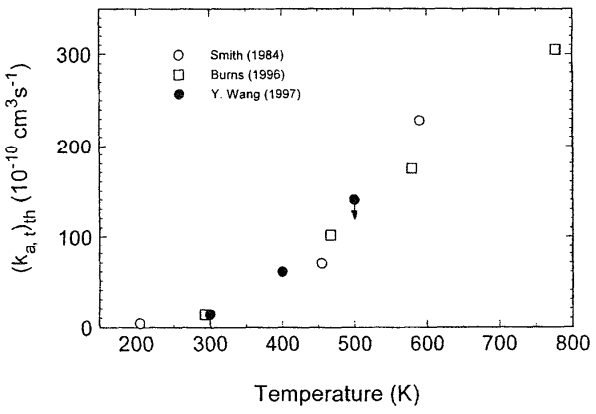

FIG. 24. Variation of the thermal value, $(k_{a,t})_{th}$, of the electron attachment rate constant for CCl_2F_2 with temperature. ○ (Ref. 85); ● (Ref. 30); □ (Ref. 92). The three sets of data were normalized to the average value of $(k_{a,t})_{th}$ at T=300 K. The downward arrow indicates an upper limit.

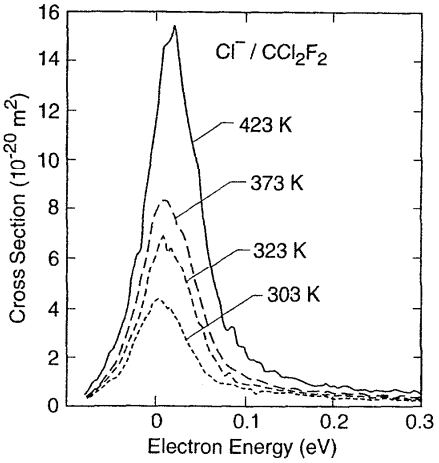

FIG. 26. Temperature dependence of the cross section for the production of Cl^- from CCl_2F_2 measured in a crossed-beam experiment (from Ref. 94).

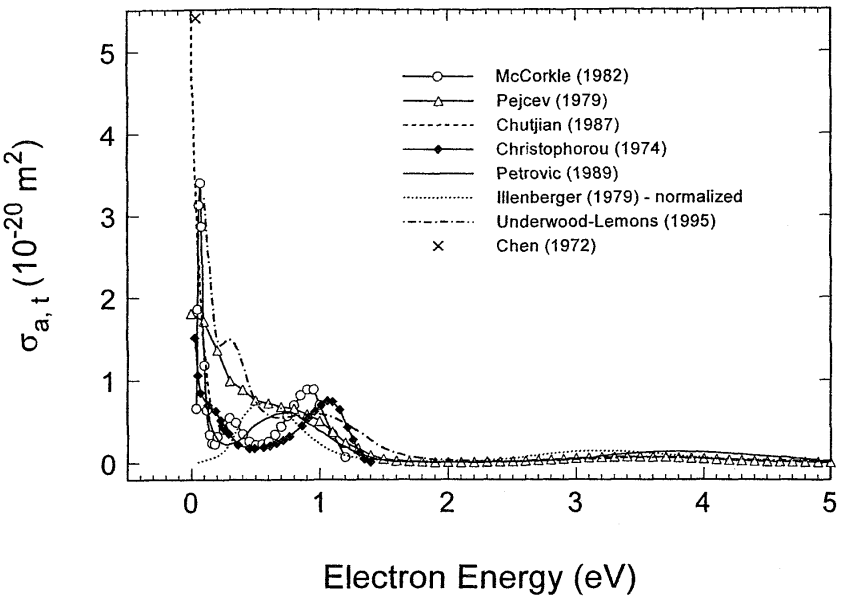

FIG. 27. Total electron attachment cross section as a function of electron energy, $\sigma_{a,t}(\varepsilon)$, for CCl_2F_2 as determined by various methods. Swarm unfolded: -○- (Ref. 27); -◆- (Ref. 26) (multiplied by 0.7, see text); — (Ref. 28). Electron beam: △ (Ref. 31); -.- (Ref. 35); × (Ref. 93). Threshold attachment: - - - (Ref. 25). In addition, the dotted line (. . . . .) shows the sum of the relative yields of all observed fragment anions detected by Illenberger *et al.* (Refs. 32–34) (see the text) normalized to the data of Ref. 31 at 0.7 eV.

system has been investigated.[99] While in this study the density of the various negative ion species has been determined by detecting the extra electrons created by laser photodetachment, other studies[100] of this general type detected Cl atoms and chlorine-containing negative ions in rf plasmas using a two-photon laser-induced fluorescence technique. In this latter method the negative ions were detected by laser photodetachment followed by two-photon excitation of the atomic chlorine, i.e., the Cl^- ions were detected by looking at the Cl atom rather than by looking at the released electron. The spatially resolved plasma concentration measurements of Selwyn *et al.*,[100] under certain etching conditions, indicated

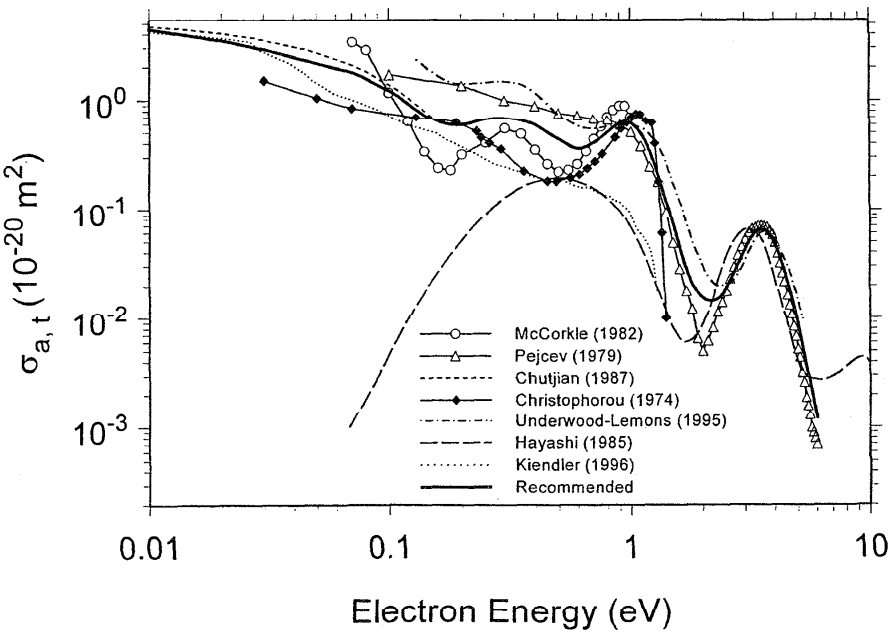

FIG. 28. Recommended total electron attachment cross section (—) for CCl_2F_2 based on an assessment of the various measurements below 0.1 eV, between 0.1 eV and 1.2 eV, and above 1.2 eV (see the text). The rest of the $\sigma_{a,t}(\varepsilon)$ plotted are from the following sources: ○ (Ref. 27); △ (Ref. 31); - - - (Ref. 25); ◆ (Ref. 26) (multiplied by 0.7, see text); -.- (Ref. 35); — — (Ref. 40); . . . . (Ref. 94).

TABLE 19. Recommended total electron attachment cross section, $\sigma_{a,t}(\varepsilon)$, for CCl_2F_2

Electron energy (eV)	$\sigma_{a,t}(\varepsilon)(10^{-20}$ m$^2)$
0.010	4.42
0.015	3.85
0.020	3.48
0.025	3.16
0.030	2.90
0.035	2.67
0.040	2.47
0.045	2.31
0.050	2.17
0.060	1.96
0.070	1.79
0.080	1.58
0.090	1.38
0.10	1.23
0.15	0.68
0.20	0.60
0.25	0.67
0.30	0.69
0.35	0.65
0.40	0.59
0.45	0.50
0.50	0.44
0.60	0.36
0.70	0.41
0.80	0.51
0.90	0.62
1.00	0.62
1.25	0.27
1.50	0.073
1.75	0.025
2.00	0.016
2.50	0.019
3.00	0.043
3.50	0.066
4.00	0.047
4.50	0.023
5.00	0.009
6.00	0.001

an anomalously large signal spike at the plasma/sheath boundary which they attributed to an aggregation of chlorine-containing negative ions.

7. Electron Transport

7.1. Electron Drift Velocity, w

There is only one measurement[101] of the electron drift velocity, w, as a function of E/N in pure CCl_2F_2. The measurements of Naidu and Prasad[101] were conducted at 293 K with an estimated uncertainty of $\pm 5\%$. Data taken off Fig. 2 of their paper (solid line) are plotted in Fig. 30 and are listed in Table 20.

7.2. Ratio of the Transverse Electron Diffusion Coefficient to Electron Mobility, D_T/μ

Two measurements[101,102] have been made of the ratio D_T/μ as a function of E/N for CCl_2F_2. These were both made at 293 K and are plotted in Fig. 31. The data plotted were taken off the solid lines of Figs. 2 of Naidu and Prasad[101] and Maller and Naidu.[102] The uncertainty quoted for both measurements is $\pm 5\%$. A fit to the two sets of measurements is shown in Fig. 31 and numerical values are listed in Table 21. Interestingly, D_T/μ increases rather slowly with increasing E/N. More measurements are needed over a wider E/N range.

Limited measurements of D_T/μ in CCl_2F_2/N_2 mixtures have been made by Maller.[103]

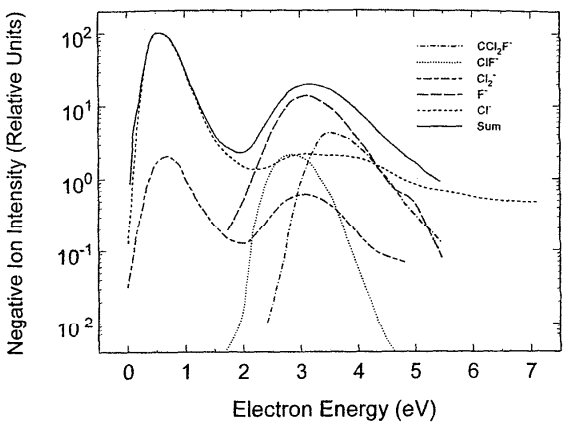

FIG. 29. Relative negative ion intensity as a function of electron energy for the production of Cl^-, F^-, Cl_2^-, ClF^-, and CCl_2F^- by electron impact on CCl_2F_2 as reported by Illenberger *et al.* (Refs. 32–34). The data have been put on a "relative absolute scale" using the energy-integrated ion intensities given by Illenberger *et al.* (Ref. 32). The solid line represents the sum of the relative absolute intensities of all the ions in the figure (see discussion in text).

7.3. Effective Ionization Coefficient $(\alpha-\eta)/N$ and $(E/N)_{lim}$

Figure 32 shows the variation with E/N of the effective ionization coefficient, $(\alpha-\eta)/N=\bar{\alpha}/N$, of CCl_2F_2. This quantity was reported by Fréchette.[69,72] We have also derived

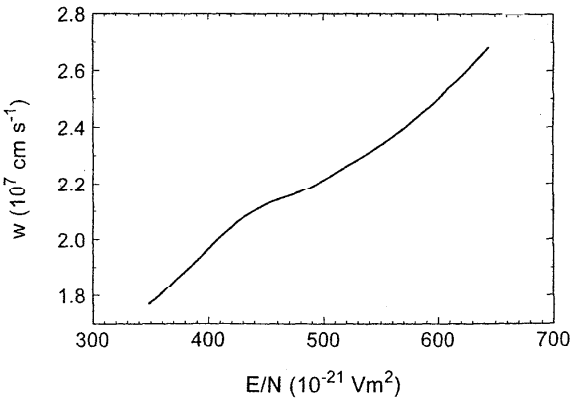

FIG. 30. Electron drift velocity, w, as a function of E/N for CCl_2F_2 ($T=293$ K) (data of Naidu and Prasad, Ref. 101).

TABLE 20. Electron drift velocity, w, in pure CCl_2F_2 as a function of E/N[a]

$E/N(10^{-21}$ V m$^2)$	$w(10^7$ cm s$^{-1})$
350	1.78
375	1.87
400	1.97
425	2.06
450	2.13
475	2.16
500	2.21
525	2.27
550	2.34
575	2.41
600	2.50
625	2.60
640	2.66

[a]Data of Naidu and Prasad (Ref. 101).

values of this quantity using our recommended values for α/N (Fig. 16) and η/N (Fig. 18) from Sec. 6, which are shown as solid circles in Fig. 32. The latter data are given in Table 22 as our recommended values.

In Table 23 are listed measurements[63–66,71,74,83,104,105] of the limiting (or critical) value, $(E/N)_{\text{lim}}$; that is, the value of E/N at which $\alpha/N=\eta/N$ ($\bar{\alpha}/N=0$) or the E/N value at which gas breakdown occurs under uniform field conditions. The average of the $(E/N)_{\text{lim}}$ values, determined from α/N and η/N measurements, listed in Table 23 is $(371\pm5)\times10^{-17}$ V cm^2.

Measurements have also been reported on the values of $(E/N)_{\text{lim}}$ for binary mixtures of CCl_2F_2 with air (Ref. 63), N_2 (Refs. 66, 67, 71, 72, 103, 104, 106), CO_2 (Refs. 74, 76, 104), and SF_6 (Refs. 106, 107), and in tertiary mixtures with SF_6/CO_2 (Ref. 108) and SF_6/N_2 (Ref. 105).

8. Optical Emission Under Electron Impact

Allcock and McConkey[109] used time-of-flight mass spectroscopy to study the electron impact induced fragmentation of CCl_2F_2 via the detection of metastable fragments. The metastable fragments they observed included C, F, Cl Rydberg atoms, fluorine atoms in the $3s^4P_{5/2}$ state, and chlorine molecules in the metastable state $c^3\Sigma_{iu}$ (excitation energy 7.2 eV). The kinetic energies of the fragments for many of the processes they studied were high, indicating steeply repulsive potential energy surfaces in the Franck–Condon region. The reaction producing the $F(^4P_{5/2})$ species has an asymptotic energy or dissociation limit (defined as the energy required to break a bond and separate the two fragments to infinite separation plus the internal excitation energy of these fragments) of 27.3 eV ±1.0 eV and was identified as

$$e + CCl_2F_2 \rightarrow CCl_2F^+ + F(^4P_{5/2}) + 2e. \quad (9)$$

They estimated a value of 14.6 eV for the appearance threshold of CCl_2F^+ based on the value of 27.3 eV for the asymptotic energy of reaction (9) and the excitation energy of 12.7 eV for $F(^4P_{5/2})$.

TABLE 21. Recommended values of D_T/μ as a function of E/N for CCl_2F_2 ($T=293$ K)

E/N (10^{-21} V m^2)	D_T/μ (V)
335	3.82
350	3.81
400	3.76
425	3.77
450	3.79
475	3.82
500	3.84
525	3.86
550	3.88
575	3.90
600	3.93
625	3.96
650	4.01
675	4.07
700	4.13
725	4.19

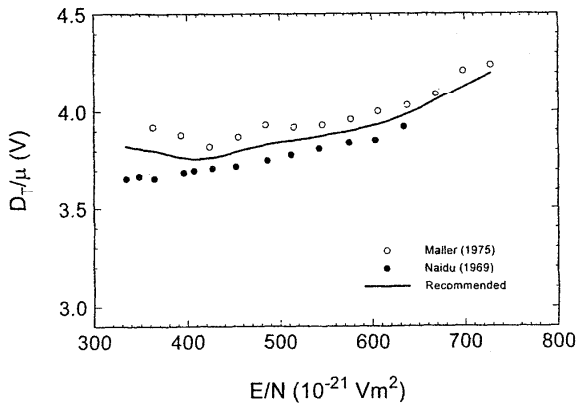

FIG. 31. D_T/μ as a function of E/N for CCl_2F_2. ● (Ref. 101); ○ (Ref. 102); — (recommended).

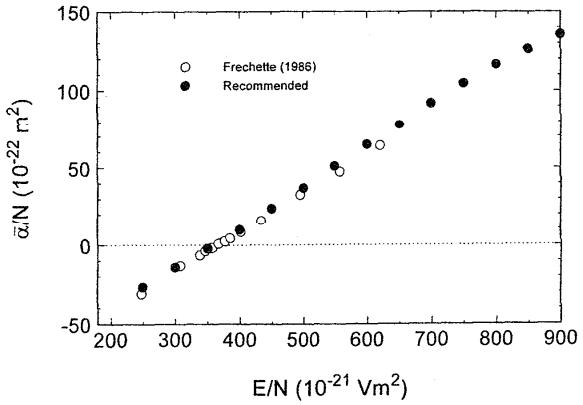

FIG. 32. Effective ionization coefficient, $\bar{\alpha}/N=(\alpha-\eta)/N$, as a function of E/N for CCl_2F_2. ○ (Ref. 69); ● (recommended) [derived from the recommended values for α/N (Fig. 16) and η/N (Fig. 18)].

TABLE 22. Recommended effective ionization coefficients, $\bar{\alpha}/N = (\alpha - \eta)/N$, for CCl_2F_2 as a function of E/N

$E/N(10^{-21}$ V m$^2)$	$\bar{\alpha}/N(10^{-22}$ m$^2)$
250	−26.4
300	−14.0
350	−2.0
400	10.0
450	24.0
500	37.0
550	51.0
600	64.8
650	77.8
700	91.8
750	104.4
800	116.5
850	126.2
900	135.6

While the study of Allcock and McConkey detected metastable fragments, it did not do so by looking at light emission. An early such study on electron impact light-induced emission from CCl_2F_2 was conducted by Van Sprang *et al.*[110] The emission spectrum they observed using 100 eV incident energy electrons exhibited emission lines of atomic fragments at long wavelengths and continuous emission, with diatomic fragment emissions superimposed, at the short wavelength side. Figure 33 shows the emission spectrum they observed in the wavelength range 2000–4400 Å. It contains emission from diatomic fragments, pronounced emission at 2367 Å from the CCl^+ ionic species, and superimposed continuous radiation. The continuous emission has an estimated threshold of 15.7±0.5 eV and was ascribed to the $CF_2Cl_2^+$ $(E^2B_1 - A^2B_1)$ transition (see Van Sprang *et al.* for the energy dependence of the continuum emission cross section). In Table 24 are listed the emission cross sections, σ_{em}(100 eV), measured by Van Sprang *et al.* using electrons with 100 eV incident energy, for the various F and Cl atomic lines. The uncertainty of these measurements was quoted to be about ±10%.

More recently, Jabbour and Becker,[111] analyzed the optical emissions in the wavelength region 2000–8000 Å produced by dissociative electron impact on CCl_2F_2. They determined absolute photoemission cross sections for a variety of neutral and ionic fluorine and chlorine lines as well as for the strong CCl and CCl^+ bands at 2778 Å and 2368 Å, respectively. Absolute photoemission cross sections at 100 eV energy for the most intense lines are given in Table 24 where they are compared with the data of Van Sprang *et al.*[110] The overall agreement between the cross section values of the two groups is good, although the cross sections of Jabbour and Becker[111] are generally smaller by about 15%. The wavelength region between 4000 Å and 6000 Å was found to be dominated by ionic fluorine and chlorine emissions and by atomic chlorine lines corresponding to the $5p \rightarrow 4s$ manifold. From a comparison of the calculated minimum energies required for the formation of excited F*(3p) and Cl*(4p) fragments via several partial and total fragmentation channels and the measured appearance potentials, they concluded that the total fragmentation of the parent molecule is the most probable dissociation channel, viz.

$$CCl_2F_2 \rightarrow C + 2\,Cl + F + F^*(3p)(31.2\,eV), \quad (10)$$

$$CCl_2F_2 \rightarrow C + 2\,F + Cl + Cl^*(4p)(27.1\,eV). \quad (11)$$

The wavelength region 2000–4000 Å showed several structured emissions superimposed on a continuum. The most prominent structured emissions were identified as arising from diatomic fragments, the $A^2\Delta \rightarrow X^2\Pi$ system of CCl centered at 2778 Å and the CCl^+ emission at 2368 Å assigned to the $A^1\Pi \rightarrow X^1\Sigma$ transition. On energetic grounds, Jabbour and Becker[111] concluded that the excited CCl^+ fragments are the result of a breakup of the parent CCl_2F_2 molecule with simultaneous formation of atomic ground state chlorine and fluorine atoms, viz.,

$$CCl_2F_2 \rightarrow CCl^+(A^1\Pi) + Cl + 2\,F(31.2\,eV) + e \quad (12)$$

and the $CCl(A^2\Delta)$ via the channel

$$CCl_2F_2 \rightarrow CCl(A^2\Delta) + Cl + 2\,F(17.6\,eV). \quad (13)$$

(See Ref. 111 for ionic chlorine and fluorine emissions in the range 3500–4000 Å.)

With regard to the continuous emission, Jabbour and Becker[111] determined its onset to be 14.2±1.0 eV which is close to the vertical ionization onset of the D^2B_2 state of $CCl_2F_2^+$ parent ion of 14.4 eV. Consequently, they assigned

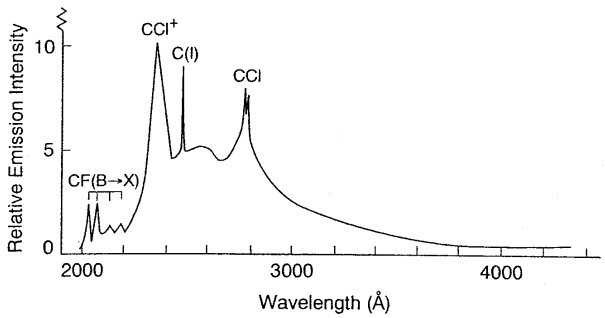

FIG. 33. Electron-impact-induced emission spectrum of CCl_2F_2 in the wavelength range 2000–4400 Å (data of Van Sprang *et al.*, Ref. 110).

TABLE 23. $(E/N)_{lim}$ for CCl_2F_2

$(E/N)_{lim}(10^{-17}$ V cm$^2)$	Reference
360[a]	74
372[a]	71
372[a]	65
373[a]	64
373[a]	66
375[a]	63
357	105
379	104
390	83

[a]These are the values of $(E/N)_{lim}$ determined from values of E/N at which $\alpha/N = \eta/N$; the rest of the data are from uniform field breakdown measurements.

TABLE 24. Emission cross sections, σ_{em} (100 eV), for various atomic F and Cl lines, resulting from the impact of 100 eV electrons on CCl_2F_2

Line	Wavelength (Å)[a]	σ_{em} (10^{-19} cm^2) Ref. 110	Ref. 111
F(I)$^2P_0$ - ^2P	7037	0.9	0.9
	7127	1.0	0.5
	7202*	—	0.3
F(I)$^2D_0$ - ^2P	7607	0.6	—
	7754	3.1	2.7
	7800	1.7	1.6
F(I)$^2S_0$ - ^2P	7311	1.6	—
F(I)$^4P_0$ - ^4P	7331	1.5	—
	7398	2.8	2.8
	7425	0.6	0.6
F(I)$^4D_0$ - ^4P	6773	1.4	0.6
	6795*	—	0.1
	6834*	—	0.9
	6856	5.1	3.5
	6870*	—	0.7
	6902	3.5	2.0
	6910*	—	0.7
F(I)$^4S_0$ - ^4P	6240*	—	0.9
	6349*	—	0.6
	6413*	—	0.4
Cl(I)$^4D_0$ - ^4P	8212	9.0	
	8333	4.5	
	8375	29	
	8428	3.1	
	8586	12	
Cl(I)$^4S_0$ - ^4P	7256	2.0	2.0
	7546	2.6	2.8
	7745*	—	0.6

[a]The wavelength numbers are from Van Sprang *et al.* (Ref. 110) except for those indicated by an asterisk which are from Jabbour and Becker (Ref. 111).

the continuous emission to the optically allowed $CCl_2F_2^+$ ($D^2B_2 \rightarrow X^2B^2$) transition. This assignment differs from the assignment of Van Sprang *et al.*[110] and both assignments differ from the assignment of Creasey *et al.*[112] who studied fluorescence processes in CCl_2F_2 following electron impact, He and Ne metastable impact, and vacuum UV photons for excitation. According to Creasey *et al.*[112] the broad emission centered at 2700 Å should be assigned to the $CF_2A^1B_1 \rightarrow X^1A_1$ transition of the CF_2 radical and not to electronic transitions in the parent molecular ion. They did not observe parent ion emission. Creasey *et al.* reported that the emission spectrum they recorded from electron impact on supersonic molecular beam of CCl_2F_2 was similar to the room temperature electron impact spectrum of Van Sprang *et al.* and Jabbour and Becker.

Finally, Roque *et al.*[113] studied the emission of fluorine $(2p^43s)^{2,4}P \rightarrow (2p^5)^2P$ resonance lines in the vacuum ultraviolet following dissociative excitation of CCl_2F_2 by electron impact. In Fig. 34 is shown the absolute emission cross sections of the fluorine $^2P \rightarrow ^2P$ multiplet at 955 Å as a function of the electron energy. The data points are the measured apparent cross sections and the solid line is the cascade-corrected contribution due to direct excitation. Roque *et al.*[113] determined the onset of this emission to be 21.5 eV ± 1.5 eV, which is lower than the minimum energy of 29.0 eV for total fragmentation of the CCl_2F_2 molecule, viz.,

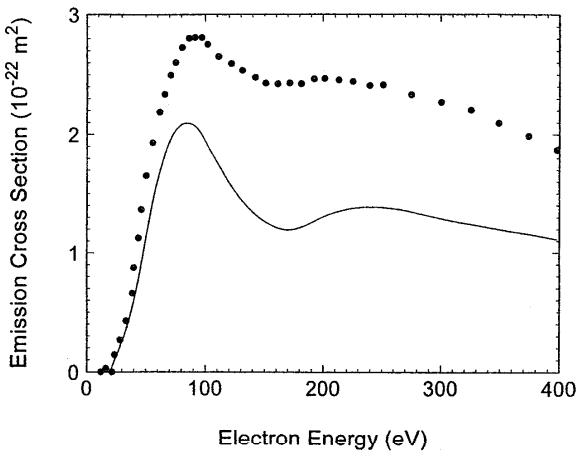

FIG. 34. Absolute emission cross section of the fluorine $^2P \rightarrow ^2P$ multiplet at 955 Å as a function of electron energy, produced by electron impact dissociative excitation of CCl_2F_2. The data points are measured apparent cross sections and the solid line is the cascade-corrected contribution due to direct excitation (data of Roque *et al.*, Ref. 113).

$$CCl_2F_2 \rightarrow C + 2Cl + F + F^*(3s^2P). \quad (14)$$

This finding, coupled with the shape of the energy dependence of the emission cross section in Fig. 34 which indicates the opening up of another dissociation channel at energies above 35 eV, led Roque *et al.* to conclude that partial fragmentation channels (e.g., $CCl_2F_2 \rightarrow CF + Cl_2 + F^*$, threshold=21.4 eV; $CCl_2F_2 \rightarrow CCl_2 + F + F^*$, threshold =22.1 eV) play an important role in the breakup of the CCl_2F_2 molecule, along with the total dissociation of the molecule via process (14).

9. Recommended Cross Sections and Transport Coefficients

In Fig. 35 are plotted the cross sections that have been derived from several sets of data, and have been designated as recommended in this article. These are

- $\sigma_{sc,t}(\varepsilon)$–Table 6, Fig. 4; and
- $\sigma_{a,t}(\varepsilon)$–Table 19, Fig. 28.

The stated uncertainties of the original data from which these cross sections have been derived vary from ±5% to ±25%.

The other three recommended cross sections plotted in Fig. 35 come from individual sources

- $\sigma_{e,int}(\varepsilon)$–Ref. 19, Table 8, Fig. 7;

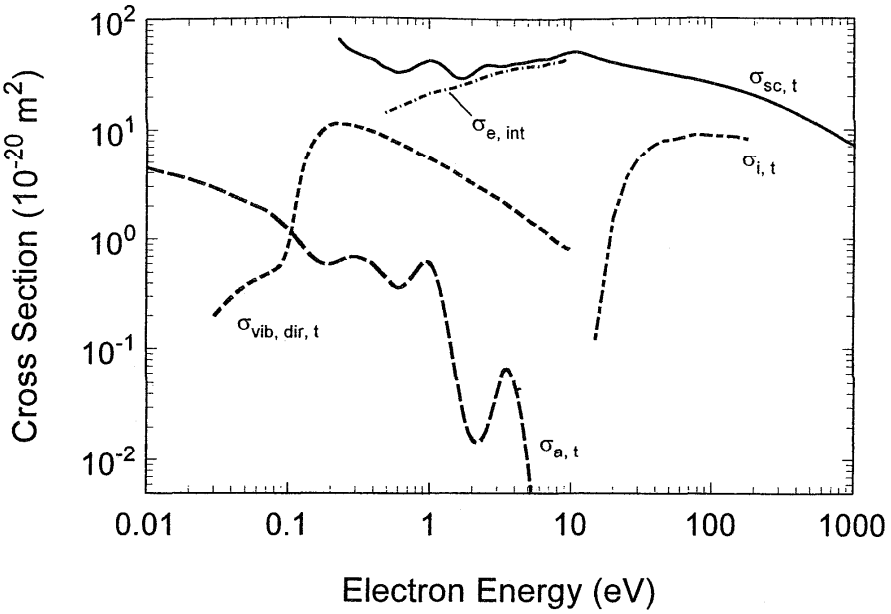

FIG. 35. Recommended cross sections (see text).

- $\sigma_{vib,\,dir,\,t}(\varepsilon)$–Ref. 19, Table 9, Fig. 9;
- $\sigma_{i,\,t}(\varepsilon)$–Ref. 49, Table 10, Fig. 13. (These data were selected over other experimental measurements for the reasons discussed in Section 4.1.)

In addition to the cross sections presented in Fig. 35, the partial (Table 11, Fig. 14) and double (Table 13, Fig. 15) ionization cross section data of Leiter *et al.*[49] are recommended in the absence of any other measurements.

Our recommended data for the electron attachment rate constant, electron attachment coefficient, ionization coefficient, effective ionization coefficient, and ratio of lateral diffusion coefficient to mobility are as follows based on the discussion in the text:

- $k_{a,\,t}$ (Table 16, Fig. 22)
- η/N (Table 15, Fig. 18)
- α/N (Table 14, Fig. 16)
- $(\alpha-\eta)/N$ (Table 22, Fig. 32)
- D_T/N (Table 21, Fig. 31).

The stated uncertainties for the coefficient data from which our recommended values have been derived range from $\pm 3\%$ to $\pm 15\%$. There is only one set of measurements of the electron drift velocity, w (Table 20, Fig. 30).

10. Conclusions

The present critically evaluated synthesis of the available information on cross sections and rate coefficients for collisional interactions of low energy electrons with dichlorodifluoromethane has led to a reasonably complete set of cross sections and transport data, in spite of the fact that the available data are limited, particularly for electron collision cross sections. The recommended data can form the basis of Boltzmann and Monte Carlo calculations to determine model-dependent collision cross section sets for this molecule. Such information is also needed.

There is a need for additional experimental measurements on a wide range of electron collision processes for this molecule, foremost electron-impact cross sections for momentum transfer and dissociation of CCl_2F_2 into neutral species. Also, the cross section $\sigma_{e,\,int}(\varepsilon)$ needs to be measured over an expanded energy range and the cross section $\sigma_{vib,\,indir,t}(\varepsilon)$ needs experimental confirmation. Moreover, since most of the recommended cross sections have been derived from limited or from single measurements, they merit confirming experiments.

The recommended data for this molecule, and for CF_4 (Ref. 5) and CHF_3 (Ref. 43) can be found on the WWW at *http://www.eeel.nist.gov/811/refdata.*

11. Acknowledgments

The authors wish to thank J. Verbrugge for valuable assistance with the literature and R. J. Van Brunt, M. V. V. S. Rao, J. Moore, and J. A. Tossell for valuable discussions. This research has been sponsored in part by the U.S. Air Force Wright Laboratory under Contract No. F3361596-C-2600 with the University of Tennessee.

[1] G. Smolinsky, R. P. Chang, and T. M. Mayer, J. Vac. Sci. Technol. **18**, 12 (1981).
[2] F. S. Rowland and M. J. Molina, Rev. Geophys. Space Phys. **13**, 1 (1975).
[3] F. S. Rowland, Environ. Conservation **15**, 101 (1988).
[4] The 1994 Report of the Scientific Assessment Working Group of IPCC, Intergovernmental Panel on Climate Change, p. 28.
[5] L. G. Christophorou, J. K. Olthoff, and M. V. V. S. Rao, J. Phys. Chem. Ref. Data **25**, 1341 (1996).

[6] W. Zhang, G. Cooper, T. Ibuki, and C. E. Brion, Chem. Phys. **151**, 357 (1991).
[7] T. Cvitaš, H. Güsten, and L. Klasinc, J. Chem. Phys. **67**, 2687 (1977).
[8] A. W. Potts, I. Novak, F. Quinn, G. V. Marr, B. Dobson, I. H. Hillier, and J. B. West, J. Phys. B **18**, 3177 (1985).
[9] A. L. McClellan, *Tables of Experimental Dipole Moments* (W. H. Freeman, San Francisco, CA, 1963), p. 35.
[10] J. A. Beran and L. Kevan, J. Phys. Chem. **73**, 3860 (1969).
[11] H. W. Jochims, W. Lohr, and H. Baumgärtel, Ber. Bunsenges. Phys. Chem. **80**, 130 (1976).
[12] J. Doucet, P. Sauvageau, and C. Sandorfy, J. Chem. Phys. **58**, 3708 (1973).
[13] C. Y. R. Wu, L. C. Lee, and D. L. Judge, J. Chem. Phys. **71**, 5221 (1979).
[14] R. Gilbert, P. Sauvageau, and C. Sandorfy, J. Chem. Phys. **60**, 4820 (1974).
[15] G. C. King and J. W. McConkey, J. Phys. B **11**, 1861 (1978).
[16] W. Zhang, T. Ibuki, and C. E. Brion, Chem. Phys. **160**, 435 (1992).
[17] R. H. Huebner, D. L. Bushnell, Jr., R. J. Celotta, S. R. Mielczarek, and C. E. Kuyatt, Nature **257**, 376 (1975).
[18] J. C. Person, D. E. Fowler, and P. P. Nicole, Argonne National Laboratory Report ANL-75-60 Part 1, 1975 (see Ref. 16).
[19] A. Mann and F. Linder, J. Phys. B **25**, 1633 (1992).
[20] T. Shimanouchi, J. Phys. Chem. Ref. Data **3**, 269 (1974).
[21] H. Dispert and K. Lacmann, Int. J. Mass Spectrom. Ion Phys. **28**, 49 (1978).
[22] H. J. T. Preston and J. J. Kaufman, Chem. Phys. Lett. **50**, 157 (1977).
[23] J. J. Kaufman, H. E. Popkie, and H. J. T. Preston, Int. J. Quantum Chem. **XI**, 1005 (1977).
[24] J. A. Tossell (private communication, October, 1996).
[25] A. Chutjian and S. H. Alajajian, J. Phys. B **20**, 839 (1987).
[26] L. G. Christophorou, D. L. McCorkle, and D. Pittman, J. Chem. Phys. **60**, 1183 (1974).
[27] D. L. McCorkle, A. A. Christodoulides, L. G. Christophorou, and I. Szamrej, J. Chem. Phys. **72**, 4049 (1980).
[28] Z. Lj. Petrovič, W. C. Wang, and L. C. Lee, J. Chem. Phys. **90**, 3145 (1989).
[29] W. C. Wang and L. C. Lee, IEEE Trans. Plasma Science **PS-15**, 460 (1987).
[30] Y. Wang and L. G. Christophorou, J. Chem Phys. (to be published).
[31] V. M. Pejčev, M. V. Kurepa, and I. M. Čadež, Chem. Phys. Lett. **63**, 301 (1979).
[32] E. Illenberger, H.-U. Scheunemann, and H. Baumgärtel, Chem. Phys. **37**, 21 (1979).
[33] E. Illenberger, Ber. Bunsenges. Phys. Chem. **86**, 252 (1982).
[34] T. Oster, A. Kühn, and E. Illenberger, Int. J. Mass Spectrom. Ion Processes **89**, 1 (1989).
[35] T. Underwood-Lemons, T. J. Gergel, and J. H. Moore, J. Chem. Phys. **102**, 119 (1995).
[36] G. J. Verhaart, W. J. van der Hart, and H. H. Brongersma, J. Chem. Phys. **34**, 161 (1978).
[37] R. K. Jones, J. Chem. Phys. **84**, 813 (1986).
[38] T. Underwood-Lemons, D. C. Winkler, J. A. Tossell, and J. H. Moore, J. Chem. Phys. **100**, 9117 (1994).
[39] P. D. Burrow, A. Modelli, N. S. Chiu, and K. D. Jordan, J. Chem. Phys. **77**, 2699 (1982).
[40] M. Hayashi, in *Swarm Studies and Inelastic Electron-Molecule Collisions*, edited by L. C. Pitchford, B. V. McKoy, A. Chutjian, and S. Trajmar (Springer, New York, 1987), p. 167.
[41] A. Zecca, G. P. Karwasz, and R. S. Brusa, Phys. Rev. A **46**, 3877 (1992).
[42] Y. Jiang, J. Sun, and L. Wan, Phys. Rev. A **52**, 398 (1995).
[43] L. G. Christophorou, J. K. Olthoff, and M. V. V. S. Rao, J. Phys. Chem. Ref. Data **26**, 1 (1997).
[44] H. -X. Wan, J. H. Moore, J. K. Olthoff, and R. J. Van Brunt, Plasma Chem. Plasma Process. **13**, 1 (1993).
[45] J. P. Novak and M. F. Fréchette, J. Appl. Phys. **57**, 4368 (1985).
[46] K. Rohr, *Proceedings of the 11th International Conference on Physics of Electronic and Atomic Collisions, Kyoto* (North Holland, Amsterdam, 1979), Abstracts, p. 322, and unpublished results quoted in Ref. 19.
[47] J. Randell, J.-P. Ziesel, S. L. Lunt, G. Mrotzek, and D. Field, J. Phys. B **26**, 3423 (1993).
[48] J. A. Beran and L. Kevan, J. Phys. Chem. **73**, 3866 (1969).
[49] K. Leiter, P. Scheier, G. Walder, and T. D. Märk, Int. J. Mass Spectrom. Ion Processes **87**, 209 (1989).
[50] D. Rapp and P. Englander-Golden, J. Chem. Phys. **43**, 1464 (1965).
[51] T. D. Märk (private communication, February 1997).
[52] H. Deutsch, P. Scheier, and T. D. Märk, Intern. J. Mass Spectrom. Ion Processes **74**, 81 (1986).
[53] G. Elwert, Z. Naturforsch. **7A**, 432 (1952).
[54] L. Vriens, Phys. Rev. **141**, 88 (1966).
[55] M. Gryzinski, Phys. Rev. A **138**, 305 (1965).
[56] W. Lotz, Z. Phys. **206**, 205 (1967).
[57] J. M. Ajello, W. T. Huntress, Jr., and P. Rayermann, J. Chem. Phys. **64**, 4746 (1976).
[58] F. C.-Y. Wang and G. E. Leroi, Ann. Isr. Phys. Soc. **6**, 210 (1984).
[59] R. Jadrny, L. Karlsson, L. Mattsson, and K. Siegbahn, Phys. Scr. **16**, 235 (1977).
[60] W. Kischlat and H. Morgner, J. Electron Spectrosc. Relat. Phenom. **35**, 273 (1985).
[61] K. Watanabe, T. Nakayama, and J. Mottl, J. Quant. Spectrosc. Radiat. Transfer **2**, 369 (1962).
[62] H. Schenk, H. Oertel, and H. Baumgärtel, Ber. Bunsenges. Phys. Chem. **83**, 683 (1979).
[63] C. R. Rao and G. R. G. Raju, Int. J. Electron. **35**, 49 (1973).
[64] J. L. Moruzzi, Br. J. Appl. Phys. **14**, 938 (1963).
[65] H. A. Boyd, G. C. Crichton, and T. Munk Nielsen, IEE Conference Publication No. 70, 426 (1970).
[66] V. N. Maller and M. S. Naidu, IEEE Trans. Plasma Sci. **PS-3**, 49 (1975).
[67] V. N. Maller and M. S. Naidu, *Third IEE Conference on Gas Discharges, London, 1974* (IEE, Torbridge, 1974), p. 409.
[68] M. A. Harrison and R. Geballe, Phys. Rev. **91**, 1 (1953).
[69] M. F. Fréchette, J. Appl. Phys. **59**, 3684 (1986).
[70] L. G. Christophorou, *Atomic and Molecular Radiation Physics* (Wiley, New York, 1971), p. 38.
[71] M. C. Siddagangappa, C. S. Lakshminarasimha, and M. N. Naidu, J. Phys. D **16**, 763 (1983).
[72] M. F. Fréchette, J. Appl. Phys. **61**, 5254 (1987).
[73] Y. Qiu, X. Ren, and Z. Y. Liu, J. Phys. D **23**, 751 (1990).
[74] M. S. Dincer and G. R. G. Raju, IEEE Trans. Electr. Insul. **EI-20**, 595 (1985).
[75] Y. Qiu and X. Weng, J. Phys. D **20**, 1203 (1987).
[76] Y. Qiu, X. Ren, Z. Y. Liu, and M. C. Zhang, J. Phys. D **22**, 1553 (1989).
[77] I. Szamrej, W. Tchórzewska, H. Kość, and M. Forys, Radiat. Phys. Chem. **47**, 269 (1996).
[78] K. M. Bansal and R. W. Fessenden, J. Chem. Phys. **59**, 1760 (1973).
[79] K. G. Mothes, E. Schultes, and R. N. Schindler, J. Phys. Chem. **76**, 3758 (1972).
[80] R. Schumacher, H.-R. Sprünken, A. A. Christodoulides, and R. N. Schindler, J. Phys. Chem. **82**, 2248 (1978).
[81] C. J. Marotta, C. Tsai, and D. L. McFadden, J. Chem. Phys. **91**, 2194 (1989).
[82] L. G. Christophorou, Chem. Rev. **76**, 409 (1976).
[83] L. G. Christophorou, R. A. Mathis, D. R. James, and D. L. McCorkle, J. Phys. D **14**, 1889 (1981).
[84] D. Smith and P. Španěl, Adv. At. Mol. Opt. Phys. **32**, 307 (1994).
[85] D. Smith, N. G. Adams, and E. Alge, J. Phys. B **17**, 461 (1984).
[86] P. Popp, J. Leonhardt, and J. I. Baumbach, Radiat. Phys. Chem. **26**, 567 (1985).
[87] W. E. Wentworth, R. George, and H. Keith, J. Chem. Phys. **51**, 1791 (1969).
[88] A. A. Christodoulides, D. L. McCorkle, and L. G. Christophorou, in *Electron Molecule Interactions and Their Applications*, edited by L. G. Christophorou (Academic, New York, 1984), Vol. 2, Ch. 6.
[89] L. G. Christophorou, D. L. McCorkle, and A. A. Christodoulides, in *Electron Molecule Interactions and Their Applications*, edited by L. G. Christophorou (Academic, New York, 1984), Vol. 1, Ch. 6.
[90] S. M. Spyrou and L. G. Christophorou, J. Chem. Phys. **82**, 2620 (1985).
[91] P. G. Datskos, L. G. Christophorou, and J. G. Carter, J. Chem. Phys. **97**, 9031 (1992).
[92] S. J. Burns, J. M. Matthews, and D. L. McFadden, J. Phys. Chem. **100**, 19436 (1996).
[93] C. L. Chen and P. J. Chantry, Bull. Am. Phys. Soc. **17**, 1133 (1972).
[94] A. Kiendler, S. Matejcik, J. D. Skalny, A. Stamatovic, and T. D. Märk, J. Phys. B **29**, 6217 (1996).

[95] Von O. Rosenbaum and H. Neuert, Z. Naturforsch. **9a**, 990 (1954).
[96] W. M. Hickam and D. Berg, Adv. Mass Spectrometry **1**, 458 (1959).
[97] E. Stoffels, W. W. Stoffels, D. Vender, G. M. W. Kroesen, and F. J. de Hoog, J. Vac. Sci. Technol. A **13**, 2051 (1995).
[98] G A. Askaryan, G. M. Batanov, A. E. Barkhudarov, S. I. Gritsinin, E. G. Korchagina, I. A. Kossyi, V. P. Silakov, and N. M. Tarasova, J. Phys. D **27**, 1311 (1994).
[99] G. M. W. Kroesen, W. W. Stoffels, E. Stoffels, M. Haverlag, J. H. W. G. den Boer, and F. J. de Hoog, Plasma Sources Sci. Technol. **3**, 246 (1994).
[100] G. S. Selwyn, L. D. Baston, and H. H. Sawin, Appl. Phys. Lett. **51**, 898 (1987).
[101] M. S. Naidu and A. N. Prasad, Brit. J. Appl. Phys. **2**, 1431 (1969).
[102] V. N. Maller and M. S. Naidu, IEEE Trans. Plasma Sci. **PS-3**, 205 (1975).
[103] V. N. Maller, IEEE-IAS Annual Meeting, New York, 1978, pp. 243–246.
[104] R. S. Nema, S. V. Kulkarni, and E. Husain, IEEE Trans. Electr. Insul. **EI-17**, 434 (1982).
[105] R. E. Wootton, S. J. Dale, and N. J. Zimmerman, in *Gaseous Dielectrics II*, edited by L. G. Christophorou (Pergamon, New York, 1980), p. 137.
[106] R. J. Van Brunt, J. Appl. Phys. **61**, 1773 (1987).
[107] G. R. G. Raju and R. Hackam, J. Appl. Phys. **53**, 5557 (1982).
[108] D. Raghavender and M. S. Naidu, Fifth International Symposium on High Voltage Engineering, Braunschweig, Germany, 24–28 August, 1987, paper 15.14.
[109] G. Allcock and J. W. McConkey, J. Phys. B **11**, 741 (1978).
[110] H. A. Van Sprang, H. H. Brongersma, and F. J. De Heer, Chem. Phys. **35**, 51 (1978).
[111] Z. J. Jabbour and K. Becker, J. Chem. Phys. **90**, 4819 (1989).
[112] J. C. Creasey, I. R. Lambert, R. P. Tuckett, and A. Hopkirk, Mol. Phys. **71**, 1367 (1990).
[113] M. B. Roque, R. B. Siegel, K. E. Martus, V. Tarnovsky, and K. Becker, J. Chem. Phys. **94**, 341 (1991).